

A Streamline-Upwind Petrov-Galerkin Finite Element Scheme for the Thermochemical Nonequilibrium Navier-Stokes Equations Part I: Non-Ionized Flows

Benjamin S. Kirk* and Steven W. Bova

NASA Lyndon B. Johnson Space Center, Houston, TX, 77058

Sandia National Laboratories, Albuquerque, NM, 87185

KEY WORDS: SUPG, finite element, compressible flows, shock capturing, inviscid flux discretization, validation

SUMMARY

This paper considers the streamline-upwind Petrov-Galerkin (SUPG) method applied to the thermochemical nonequilibrium Navier-Stokes equations in conservation-variable form. The governing equations for a non-ionized reacting mixture of perfect gases in thermal nonequilibrium are reviewed. The spatial discretization, time discretization, and solution scheme are briefly discussed. The performance of the formulation is then investigated by considering a number of classical benchmark problems in reacting flows. Mesh and iterative convergence are studied in detail for the case of inviscid, dissociating nitrogen flow about a circular cylinder. The performance of various linearization strategies is also examined in this context. Copyright © 2000 John Wiley & Sons, Ltd.

1. Introduction

At hypersonic speeds, atmospheric cruise and entry vehicles experience effects which depart considerably from the familiar calorically perfect gas regime. At flight speeds above Mach 5, the nitrogen and oxygen molecules become vibrationally excited, and the gas becomes thermally perfect. As the freestream Mach number is increased further, molecular oxygen begins to dissociate. The resulting atomic oxygen is then free to react with the molecular nitrogen, and nitric oxide may be formed. At still higher speeds (in excess of Mach 15) the nitrogen molecules begin to dissociate. At speeds above Mach 25 the gas becomes weakly ionized [1].

When the time scale associated with chemical reactions in the flow is much less than the fluid dynamic time scales, $t_{\text{chem}} \ll t_{\text{flow}}$, the gas can be assumed to be in equilibrium. In this situation the equilibrium principle holds and the state of the gas is uniquely determined by any two independent thermodynamic properties. Conversely, when the time scale associated with chemical reactions is much greater than the fluid dynamic time scales, $t_{\text{chem}} \gg t_{\text{flow}}$, the gas is said to be frozen. In this case the chemical composition of the gas is fixed throughout the domain.

*Correspondence to: Mail Code EG3, 2101 NASA Parkway, Houston, TX 77058

Between these two extremes is the regime of chemical nonequilibrium. In this case chemical and fluid dynamic time scales are comparable. The chemical composition at any point in the domain is then not only a function of local conditions but also of the streamline history. Conceptually, the gas will begin to adjust to reach an equilibrium state, but before this process has completed it will have convected downstream. It will then seek a new equilibrium state dictated by the local conditions. In this situation $t_{\text{chem}} \approx t_{\text{flow}}$, and the chemical composition of the gas itself must be determined. In this regime the flow is said to be in *chemical nonequilibrium*. For applications of interest in aerospace engineering, these flows can be modeled to good approximation by a chemically reacting mixture of perfect gases. Note this approach assumes that intermolecular forces are negligible and hence each chemical species in the flow obeys the perfect gas law, an assumption which is generally valid, except for very high pressures at low temperature [1].

Considering a diatomic molecule, it is clear that there are four possible *modes* in which the molecule may store energy:

1. Translational energy due to random motion,
2. Rotational energy due to rotation about its center of mass,
3. Vibrational energy due to relative motion between the atoms, and
4. Electronic energy due to the state of the electrons.

When the molecule is in thermal equilibrium, each of these four modes are in equilibrium with each other, and all modes can adequately be described by a single temperature T . When the gas is not in thermal equilibrium, however, each energy mode is potentially distinct and must be characterized by its own temperature, T_t, T_r, T_v, T_e . Further, each molecular species in the gas may be characterized by its own vibrational temperature [2].

The mechanism by which the energy modes are equilibrated is through collisions. It is traditionally assumed that the translational and rotational modes equilibrate very rapidly (within $\mathcal{O}(5 - 10)$ collisions [2, 3]), therefore they may be modeled with a single translational/rotational temperature $T \equiv T_t = T_r$. It is worth noting that recent research may refute this assumption for the case of nitrogen passing through a very strong shock [4], suggesting that this assumption may need to be revisited in the future.

By contrast, the vibrational modes require many more collisions to equilibrate. As in the case of chemical nonequilibrium, it is entirely possible that during the process of vibrational equilibration the gas will convect downstream with a different equilibrium vibrational state [1]. In this situation we must consider the vibrational energy as separate and distinct from the translational/rotational modes. One common assumption, which we adopt here, is to model the vibrational and electronic temperatures with the same temperature $T_V \equiv T_v = T_e$ [5]. We thus arrive at a two-temperature system for the case of thermal nonequilibrium.

The remainder of this paper is outlined as follows. Section 2 reviews the compressible Navier-Stokes equations for a reacting mixture of perfect gases in thermal nonequilibrium. Section 3 then presents the stabilized weak form of the governing equations and describes the associated finite element discretization. The parallel solution methodology is briefly described in Section 5, and the performance of the algorithm is then investigated with numerical experiments and validation cases in Section 6. Finally, some general observations are drawn and areas for future research are discussed in Section 7.

2. Mathematical Model

The compressible Navier–Stokes equations describe the conservation of mass, momentum, and energy for this class of flows. This section summarizes the Navier–Stokes system of equations, relevant state equations and transport property models for air, and the nondimensionalization scheme used in the present work.

2.1. Conservation Equations

The conservation of mass, momentum, and total energy for a compressible fluid composed of ns constitutive components may be written as

$$\frac{\partial \rho_s}{\partial t} + \nabla \cdot \rho_s (\mathbf{u} + \mathbf{u}_s) = \dot{\omega}_s \quad (1)$$

$$\frac{\partial \rho \mathbf{u}}{\partial t} + \nabla \cdot (\rho \mathbf{u} \mathbf{u}) = -\nabla P + \nabla \cdot \boldsymbol{\tau} \quad (2)$$

$$\frac{\partial \rho E}{\partial t} + \nabla \cdot (\rho H \mathbf{u}) + \nabla \cdot \left(\sum_{s=1}^{ns} \rho_s \mathbf{u}_s h_s \right) = -\nabla \cdot \dot{\mathbf{q}} + \nabla \cdot (\boldsymbol{\tau} \mathbf{u}) \quad (3)$$

where ρ_s is the density of species s , $\rho = \sum_s \rho_s$ is the mixture density, \mathbf{u} is the mixture velocity, \mathbf{u}_s is the diffusion velocity of species s , E is the total energy per unit mass, and P is the pressure. The total enthalpy, H , may be expressed in terms of the total energy, density, and pressure: $H = E + P/\rho$. The viscous stress tensor $\boldsymbol{\tau}$ and the heat flux vector $\dot{\mathbf{q}}$ are defined as

$$\boldsymbol{\tau} = \mu \left(\nabla \mathbf{u} + \nabla^T \mathbf{u} \right) - \frac{2}{3} \mu (\nabla \cdot \mathbf{u}) \mathbf{I} \quad (4)$$

$$\dot{\mathbf{q}} = -k \nabla T - k_v \nabla T_v - k_e \nabla T_e \quad (5)$$

where μ is the dynamic viscosity, k is the thermal conductivity, T, T_v, T_e are respectively the fluid translational/rotational, vibrational, and electron/electronic excitation temperatures, and \mathbf{I} denotes the identity matrix.

For flows in which thermal equilibrium holds, the same temperature $T = T_v = T_e$ governs all energy modes. However, for many applications in hypersonic flows, thermal equilibrium does not exist. This is because of the relatively large number of collisions required to equilibrate the vibrational energies of molecules. In general vibrational states require an order of magnitude or more collisions to equilibrate than translational/rotational states. Recognizing this, a common approach is to assume a *two temperature* model in which the translational/rotational energy is governed by the the temperature, T , while the vibrational and electronic energy are governed by a separate temperature $T_V = T_v = T_e$. In this situation the vibrational/electronic energy are governed by a separate transport equation:

$$\frac{\partial \rho e_V}{\partial t} + \nabla \cdot (\rho e_V \mathbf{u}) + \nabla \cdot \left(\sum_{s=mol} \rho_s e_{V_s} \mathbf{u}_s \right) = -\nabla \cdot \dot{\mathbf{q}}_V + \dot{\omega}_V \quad (6)$$

where the term $\sum_{s=mol}$ denotes the sum is taken over molecules. For the two-temperature model applied to a non-ionized flow the vibrational heat flux is given by $\dot{\mathbf{q}}_V = -k_v \nabla T_V$.

In general, the species diffusion velocities \mathbf{u}_s result from gradients in species concentration, temperature, and pressure. However, for most flows of interest in aerospace applications, only the species concentration term is significant. We adopt this assumption in this work, therefore species

diffusion is driven solely by concentration gradients. Under this assumption the species diffusion velocities are given by Fick's law as

$$\rho_s \mathbf{u}_s = -\rho \mathcal{D}_s \nabla c_s \quad (7)$$

where $c_s = (\rho_s/\rho)$ is the mass fraction of species s . Combining Equations (1)–(6) with (7) yields the following set of equations:

$$\frac{\partial \rho_s}{\partial t} + \nabla \cdot (\rho_s \mathbf{u}) = \nabla \cdot (\rho \mathcal{D}_s \nabla c_s) + \dot{\omega}_s \quad (8)$$

$$\frac{\partial \rho \mathbf{u}}{\partial t} + \nabla \cdot (\rho \mathbf{u} \mathbf{u}) = -\nabla P + \nabla \cdot \boldsymbol{\tau} \quad (9)$$

$$\frac{\partial \rho E}{\partial t} + \nabla \cdot (\rho H \mathbf{u}) = -\nabla \cdot \dot{\mathbf{q}} + \nabla \cdot \left(\rho \sum_{s=1}^{n_s} h_s \mathcal{D}_s \nabla c_s \right) + \nabla \cdot (\boldsymbol{\tau} \mathbf{u}) \quad (10)$$

$$\frac{\partial \rho e_V}{\partial t} + \nabla \cdot (\rho e_V \mathbf{u}) = -\nabla \cdot \dot{\mathbf{q}}_V + \nabla \cdot \left(\rho \sum_{s=mol} e_{V,s} \mathcal{D}_s \nabla c_s \right) + \dot{\omega}_V \quad (11)$$

which describe the viscous flow of a chemically reacting mixture of gases in thermal nonequilibrium. The special case of thermal equilibrium is recovered simply by omitting the last equation.

The total energy, E , is composed of internal and kinetic components: $E = e^{\text{int}} + \mathbf{u} \cdot \mathbf{u}/2$. In turn, the total internal energy, e^{int} , has contribution from distinct energy *modes*. Specifically

$$e^{\text{int}} = e^{\text{trans}} + e^{\text{rot}} + e^{\text{vib}} + e^{\text{elec}} + h^0 \quad (12)$$

$$= \sum_{s=1}^{n_s} c_s e_s^{\text{trans}} + \sum_{s=mol} c_s e_s^{\text{rot}} + \sum_{s=mol} c_s e_s^{\text{vib}} + \sum_{s=1}^{n_s} c_s e_s^{\text{elec}} + \sum_{s=1}^{n_s} c_s h_s^0 \quad (13)$$

The first four terms on the right of Equation (13) represent the energy due to molecular/atomic translation, molecular rotation, molecular vibration, and electronic excitation. The final term is the heat of formation of the mixture and accounts for the energy stored in chemical bonds. To good approximation the translational and rotational states of the gas may be assumed fully populated, and under this assumption the translational/rotational energy for each species may be expressed as

$$e_s^{\text{trans}} + e_s^{\text{rot}} = e_s^{\text{tr}} = C_{v,s}^{\text{tr}} T \quad (14)$$

where the translational/rotational specific heat, $C_{v,s}^{\text{tr}}$, is given by

$$C_{v,s}^{\text{tr}} = \begin{cases} \frac{5}{2} R_s & \text{for molecules,} \\ \frac{3}{2} R_s & \text{for atoms.} \end{cases} \quad (15)$$

where R_s is the species gas constant, and $R_s = R/M_s$ where R is the universal gas constant and M_s is the species molar mass. The combined term e_s^{tr} in Equation (14) represents the energy due to random thermal translational/rotational motion of a given species.

In contrast to the translational/rotational states, the vibrational energy states are typically not fully populated. One approach for modeling the molecular vibrational energy is through analogy to a harmonic oscillator. In this approach the energy potential between molecular nuclei is modeled as a quadratic function of separation distance. Under this assumption, the vibrational energy for each molecular species can be modeled as

$$e_s^{\text{vib}} = \begin{cases} \frac{R_s \theta_{v,s}}{\exp(\theta_{v,s}/T_v) - 1} & \text{for molecules,} \\ 0 & \text{for atoms.} \end{cases} \quad (16)$$

where θ_{vs} is the species characteristic temperature of vibration and T_v is the mixture vibrational temperature.

The energy contained in the excited electronic states for a given species, e_s^{elec} , can be obtained from the assumption that they are in a Boltzmann distribution governed by the electronic excitation temperature T_e as

$$e_s^{\text{elec}} = R_s \frac{\sum_{i=1}^{\infty} \theta_{is}^{\text{elec}} g_{is} \exp(-\theta_{is}^{\text{elec}}/T_e)}{g_{0s} + \sum_{i=1}^{\infty} g_{is} \exp(-\theta_{is}^{\text{elec}}/T_e)} \quad (17)$$

Recall that for the two-temperature model the vibrational and electronic excitation temperatures are assumed to be identical, that is $T_v = T_e \equiv T_V$, and that in the case of thermal equilibrium $T_r = T_t = T_v = T_e \equiv T$.

In practice, Equation (17) can usually be omitted for non-ionized flows such as those considered in this work. Park [6] observes that electronic transitions in molecules are caused mostly by the impact of free electrons. Since there are no free electrons when there is no ionization, there will be very little electronic excitation. In the present work we choose to retain Equation (17) for completeness and to aid in future expansion to weakly ionizing flows.

Combining the terms above, it is clear that in the case of thermal nonequilibrium

$$\rho E = \frac{1}{2} \rho (\mathbf{u} \cdot \mathbf{u}) + \sum_{s=1}^{ns} \rho_s C_{v,s}^{\text{tr}} T + \rho e_V + \sum_{s=1}^{ns} \rho_s h_s^0 \quad (18)$$

where the term ρe_V is provided by Equation (11). Equation (18) may be inverted directly to find the translational/rotational temperature T , however the vibrational/electronic temperature T_V must be computed iteratively from the relation

$$\rho e_V = \sum_{s=mol} \rho_s e_s^{\text{vib}}(T_V) + \sum_{s=1}^{ns} \rho_s e_s^{\text{elec}}(T_V) \quad (19)$$

In the case of thermal equilibrium we have

$$\rho E = \frac{1}{2} \rho (\mathbf{u} \cdot \mathbf{u}) + \sum_{s=1}^{ns} \rho_s C_{v,s}^{\text{tr}} T + \sum_{s=mol} \rho_s e_s^{\text{vib}}(T) + \sum_{s=1}^{ns} \rho_s e_s^{\text{elec}}(T) + \sum_{s=1}^{ns} \rho_s h_s^0 \quad (20)$$

which is clearly nonlinear in the equilibrium temperature T . In practice, a Newton iteration is performed to determine T or T_V as required, and this procedure typically converges in 2-3 iterations.

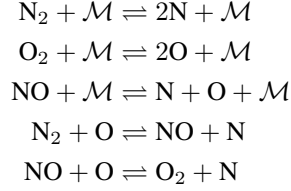
Regardless of the thermal state of the mixture, once the translational/rotational temperature T is determined the thermodynamic pressure of the mixture is readily obtained from Dalton's law of partial pressures:

$$P = \sum_{s=1}^{ns} P_s = \sum_{s=1}^{ns} \rho_s R_s T \quad (21)$$

2.2. Chemical Kinetics

The rate of production/destruction of the individual species, $\dot{\omega}_s$, is required to close the species continuity equations. To develop these relationships it is instructive to consider the case of a specific mixture. To this end, let us consider the chemical reactions which occur among the principal

components of dissociating air: N_2, O_2, NO, N, O . For this mixture the primary chemical reactions that occur are



These reactions can occur in either the forward or backward direction, as denoted by the bidirectional arrow. The reactions are presented such that they are endothermic in the forward direction. In these reactions \mathcal{M} denotes a generic collision partner, which may be any of the species present in the flow. In the case of dissociation, the collision partner provides the energy required to break the molecular bond. By contrast, during recombination the collision partner absorbs the dissociation energy from the atomic pair. The collision partner is otherwise unaltered by the reaction.

Each of the r reactions is governed by a forward and backward rate coefficient, k_{fr} and k_{br} . The rate of each reaction is therefore a sum of the forward and backward rates:

$$\begin{aligned} \mathcal{R}_1 &= \sum_{m \in \mathcal{M}} \left(k_{b1m} \frac{\rho_N}{M_N} \frac{\rho_N}{M_N} \frac{\rho_m}{M_m} - k_{f1m} \frac{\rho_{N_2}}{M_{N_2}} \frac{\rho_m}{M_m} \right) \\ \mathcal{R}_2 &= \sum_{m \in \mathcal{M}} \left(k_{b2m} \frac{\rho_O}{M_O} \frac{\rho_O}{M_O} \frac{\rho_m}{M_m} - k_{f2m} \frac{\rho_{O_2}}{M_{O_2}} \frac{\rho_m}{M_m} \right) \\ \mathcal{R}_3 &= \sum_{m \in \mathcal{M}} \left(k_{b3m} \frac{\rho_N}{M_N} \frac{\rho_O}{M_O} \frac{\rho_m}{M_m} - k_{f3m} \frac{\rho_{NO}}{M_{NO}} \frac{\rho_m}{M_m} \right) \\ \mathcal{R}_4 &= k_{b4} \frac{\rho_{NO}}{M_{NO}} \frac{\rho_N}{M_N} - k_{f4} \frac{\rho_{N_2}}{M_{N_2}} \frac{\rho_O}{M_O} \\ \mathcal{R}_5 &= k_{b5} \frac{\rho_{O_2}}{M_{O_2}} \frac{\rho_N}{M_N} - k_{f5} \frac{\rho_{NO}}{M_{NO}} \frac{\rho_O}{M_O} \end{aligned}$$

Note that each of these r reactions is of the canonical form

$$\mathcal{R}_r = \mathcal{R}_{br} - \mathcal{R}_{fr} \quad (22)$$

$$= k_{br} \prod_{s=1}^{ns} \left(\frac{\rho_s}{M_s} \right)^{\beta_{sr}} - k_{fr} \prod_{s=1}^{ns} \left(\frac{\rho_s}{M_s} \right)^{\alpha_{sr}} \quad (23)$$

where α_{sr} and β_{sr} are the stoichiometric coefficients for reactants and products of species s .

The species source terms can now be expressed in terms of the individual reaction rates as follows

$$\begin{aligned} \dot{\omega}_{N_2} &= M_{N_2} (\mathcal{R}_1 + \mathcal{R}_4) \\ \dot{\omega}_{O_2} &= M_{O_2} (\mathcal{R}_2 - \mathcal{R}_5) \\ \dot{\omega}_{NO} &= M_{NO} (\mathcal{R}_3 - \mathcal{R}_4 + \mathcal{R}_5) \\ \dot{\omega}_N &= M_N (-2\mathcal{R}_1 - \mathcal{R}_3 - \mathcal{R}_4 - \mathcal{R}_5) \\ \dot{\omega}_O &= M_O (-2\mathcal{R}_2 - \mathcal{R}_3 + \mathcal{R}_4 + \mathcal{R}_5) \end{aligned}$$

These source terms sum identically to zero, as required by conservation of mass. The source terms are of the canonical form

$$\dot{\omega}_s = M_s \sum_{r=1}^{nr} (\alpha_{sr} - \beta_{sr}) (\mathcal{R}_{br} - \mathcal{R}_{fr}) \quad (24)$$

where nr is the number of reactions.

It remains to determine the rate coefficients k_f and k_b . To this end, let us first introduce an effective temperature, \bar{T} , which is some function of the translational/rotational and vibrational temperatures. The forward rate coefficients can then be expressed in a modified Arrhenius form as

$$k_{fr}(\bar{T}) = C_{fr} \bar{T}^{\eta_r} \exp(-E_{ar}/R\bar{T}) \quad (25)$$

where C_{fr} is the reaction rate constant, η_r is the so-called pre-exponential factor, and E_{ar} is the activation energy. These three constants are determined from curve fits to experimental data. The corresponding backward rate coefficient can be found using the principle of detailed balance, which states

$$K_{eq} = \frac{k_{fr}(\bar{T})}{k_{br}(\bar{T})} \quad (26)$$

where K_{eq} is the equilibrium constant.

2.3. Vibrational Energy & Vibrational Relaxation

For the case of thermal nonequilibrium it remains to define the vibrational energy source term, $\dot{\omega}_v$, which appears in Equation (11). This term represents the production/destruction of vibrational energy in the gas, and is due to (i) the creation of molecules with some vibrational energy and (ii) the transfer of energy between the various modes in the gas. That is,

$$\dot{\omega}_v = \dot{Q}_v + \dot{Q}_{\text{transfer}} \quad (27)$$

When molecular species are created in the gas at rate $\dot{\omega}_s$, they contribute vibrational energy at the rate

$$\dot{Q}_{vs} = \dot{\omega}_s e_s^{\text{vib}}$$

so the net vibrational energy production rate is then simply

$$\dot{Q}_v = \sum_{s=\text{mol}} \dot{\omega}_s e_s^{\text{vib}} \quad (28)$$

There is also energy transfer among the various energy modes in the gas. Strictly speaking, one such energy transfer is vibration-vibration coupling between the various molecules in the gas. However, implicit in the use of a single vibrational energy equation is the assumption that the molecular vibrational energies equilibrate very rapidly and thus are adequately characterized with a single vibrational temperature T_V . There is also energy transfer between translational and vibrational modes as well as rotational and vibrational modes. These latter two exchanges are grouped together and represented as a single vibrational energy transfer rate \dot{Q}^{tr-v} .

In this work we adopt the Landau-Teller model. In this model the vibrational energy transfer for a given species is

$$\dot{Q}_s^{tr-v} = \rho_s \frac{\hat{e}_s^{\text{vib}} - e_s^{\text{vib}}}{\tau_s^{\text{vib}}} \quad (29)$$

where \hat{e}_s^{vib} is the species equilibrium vibrational energy (Equation (16) evaluated at temperature T) and the vibrational relaxation time τ_s^{vib} is given by Millikan and White

$$\tau_s^{\text{vib}} = \frac{\sum_{r=1}^{ns} \chi_r}{\sum_{r=1}^{ns} \chi_r / \tau_{sr}^{\text{vib}}} \quad (30)$$

where χ_r is given by

$$\chi_r = c_r \frac{M}{M_r}, \quad M = \left(\sum_{s=1}^{ns} \frac{c_s}{M_s} \right)^{-1} \quad (31)$$

and

$$\tau_{sr}^{\text{vib}} = \frac{1}{P} \exp \left[A_{sr} \left(T^{-1/3} - 0.015 \mu_{sr}^{1/4} \right) - 18.42 \right] \quad (32)$$

$$A_{sr} = 1.16 \times 10^{-3} \mu_{sr}^{1/2} \theta_{vs}^4 \quad (33)$$

$$\mu_{sr} = \frac{M_s M_r}{M_s + M_r} \quad (34)$$

where the pressure in Equation (32) is in units of atmospheres. Combining (29) and (28) yields the desired net vibrational energy source term

$$\dot{\omega}_V = \sum_{s=1}^{ns} \dot{Q}_s^{tr-v} + \sum_{s=mol} \dot{\omega}_s e_s^{\text{vib}} \quad (35)$$

2.4. Transport Properties

2.4.1. Species Transport Properties The viscosity for each species in the mixture can be computed using curve fits obtained by Blottner, which are of the form

$$\mu_s(T) = 0.1 \exp \left[(A_s \ln T + B_s) \ln T + C_s \right] \quad (\text{kg/m}\cdot\text{sec}) \quad (36)$$

where the constants A_s , B_s , and C_s are species dependent parameters [7,8]. These curve fits are valid for temperatures below 10,000 K, which generally speaking is sufficient for the cases considered later. At higher temperatures, or for species for which Blottner data are not available, the species transport properties can be computed using kinetic theory [9].

The thermal conductivities for the translational, rotational, and vibrational energy modes can be determined from an Eucken relation [9]. Under the assumption that the transport of translational energy is correlated to the velocity of the species (but that the transport of internal energies is not similarly correlated) the relevant thermal conductivities are

$$k_s^{\text{trans}} = \frac{5}{2} \mu_s C_{v,s}^{\text{trans}} \quad (37)$$

$$k_s^{\text{rot}} = \mu_s C_{v,s}^{\text{rot}} \quad (38)$$

$$k_s^{\text{vib}} = \mu_s C_{v,s}^{\text{vib}} \quad (39)$$

where $C_{v,s}^{\text{vib}} = \frac{\partial e_{v,s}^{\text{vib}}}{\partial T_V}$ with $e_{v,s}^{\text{vib}}$ given by Equation (16).

2.4.2. *Mixture Transport Properties* With the species viscosity and thermal conductivities computed using the above relationships, the mixture properties may be computed using Wilke’s mixing rule as follows:

$$\mu = \sum_{s=1}^{ns} \mu_s \frac{\chi_s}{\phi_s} \quad (40)$$

$$k = \sum_{s=1}^{ns} k_s \frac{\chi_s}{\phi_s} \quad (41)$$

where χ_s is as defined in Equation (31) and

$$\phi_s = \sum_{r=1}^{ns} \chi_r \frac{\left[1 + \sqrt{\frac{\mu_s}{\mu_r}} \sqrt{\frac{M_r}{M_s}} \right]^2}{\sqrt{8 \left(1 + \frac{M_s}{M_r} \right)}} \quad (42)$$

2.4.3. *Species Diffusion Coefficients* Recall from Equation (7) that the species diffusion velocities are related to the species concentration gradients through Fick’s law. In order to use this model the individual species diffusion coefficients, \mathcal{D}_s , must be determined. The multicomponent nature of the diffusion coefficients could be implemented directly, which would yield separate diffusion coefficients for each species. This approach would be required if the gas contained species with disparate molecular weights, e.g. oxygen and hydrogen. However, for the case when the constituents have similar molecular weights, it is convenient to assume a single diffusion coefficient \mathcal{D} which comes from the assumption of constant Lewis number

$$Le = \mathcal{D} \frac{\rho C_p^{\text{tr}}}{k} \quad (43)$$

where C_p^{tr} is the translational/rotational specific heat at constant pressure. For air the Lewis number is usually taken as $Le = 1.4$.

2.5. System of Equations

Equations (8)–(10) may be written in conservative system form as

$$\frac{\partial \mathbf{U}}{\partial t} + \frac{\partial \mathbf{F}_i}{\partial x_i} = \frac{\partial \mathbf{G}_i}{\partial x_i} + \dot{\mathbf{S}} \quad (44)$$

where the vector \mathbf{U} consists of the so-called conservation variables, \mathbf{F}_i and \mathbf{G}_i are the inviscid and viscous fluxes in the i^{th} direction, respectively. The conservation variables $\mathbf{U} = [\rho_s, \rho u_j, \rho E, \rho e_V]^T$ correspond to the fluid density, Cartesian components of momentum per unit volume, total energy per unit volume and vibrational/electronic energy per unit volume, respectively. The chemical species/vibrational energy source vector $\dot{\mathbf{S}} = [\dot{\omega}_s, 0, 0, \dot{\omega}_V]^T$. The inviscid and viscous fluxes in (44) are given by

$$\mathbf{F}_i = \begin{bmatrix} \rho_s u_i \\ \rho u_i u_j + \delta_{ij} P \\ \rho u_i H \\ \rho u_i e_V \end{bmatrix} \quad (45)$$

$$\mathbf{G}_i = \begin{bmatrix} 0 \\ \tau_{ij} \\ -q_i + \tau_{ij} u_j \\ 0 \end{bmatrix} \quad (46)$$

where δ_{ij} is the Kronecker delta satisfying $\delta_{ij} = 0$ when $i \neq j$ and is of unit value otherwise. In the above notation $(\)_i$ denotes the coordinate direction associated with each flux vector \mathbf{F}_i and \mathbf{G}_i . The subscript $(\)_j$ denotes the component of the momentum equation, and thus expands the length of each vector according to the spatial dimension. Similarly, $(\)_s$ denotes the chemical species index and expands each vector by the number of species in the model.

The second term on the left-hand-side of (44) is the divergence of the inviscid flux vector, $\partial \mathbf{F}_i / \partial x_i$, and may be written in terms of the unknowns \mathbf{U} as

$$\frac{\partial \mathbf{F}_i}{\partial x_i} = \frac{\partial \mathbf{F}_i}{\partial \mathbf{U}} \frac{\partial \mathbf{U}}{\partial x_i} = \mathbf{A}_i \frac{\partial \mathbf{U}}{\partial x_i} \quad (47)$$

where $\mathbf{A}_i = \partial \mathbf{F}_i / \partial \mathbf{U}$ is the inviscid flux Jacobian. Similarly, the viscous flux vector \mathbf{G}_i may be written as

$$\frac{\partial \mathbf{G}_i}{\partial x_i} = \frac{\partial}{\partial x_i} \left(\mathbf{K}_{ij} \frac{\partial \mathbf{U}}{\partial x_j} \right) \quad (48)$$

where \mathbf{K}_{ij} is a diffusivity matrix. The matrices \mathbf{A}_i and \mathbf{K}_{ij} are both functions of the independent variables \mathbf{U} and are listed explicitly in reference 10.

Using (47) and (48) in (44) yields the second-order system

$$\frac{\partial \mathbf{U}}{\partial t} + \mathbf{A}_i \frac{\partial \mathbf{U}}{\partial x_i} = \frac{\partial}{\partial x_i} \left(\mathbf{K}_{ij} \frac{\partial \mathbf{U}}{\partial x_j} \right) + \dot{\mathbf{S}} \quad (49)$$

which will be the basis for developing a weak formulation in Section 3. In the limit of vanishing viscosity the right-hand-side of Equation (49) reduces to $\dot{\mathbf{S}}$, resulting in the first-order, hyperbolic reacting Euler equations.

3. Weak Formulation

3.1. Galerkin Weak Statement

The corresponding weak form of the governing system of Equations (49) may be constructed in the standard way by first multiplying by an appropriate set of test functions \mathbf{W} and integrating over the domain Ω . Integrating the viscous term by parts yields the weak statement: Find \mathbf{U} satisfying the essential boundary and initial conditions such that

$$\int_{\Omega} \left[\mathbf{W} \cdot \left(\frac{\partial \mathbf{U}}{\partial t} + \mathbf{A}_i \frac{\partial \mathbf{U}}{\partial x_i} - \dot{\mathbf{S}} \right) + \frac{\partial \mathbf{W}}{\partial x_i} \cdot \left(\mathbf{K}_{ij} \frac{\partial \mathbf{U}}{\partial x_j} \right) \right] d\Omega - \oint_{\Gamma} \mathbf{W} \cdot \mathbf{g} d\Gamma = 0 \quad (50)$$

for all \mathbf{W} in an appropriate function space. In the last term $\mathbf{g} = \mathbf{G} \cdot \hat{\mathbf{n}}$ is the normal component of the viscous flux on the boundary Γ with unit normal $\hat{\mathbf{n}}$.

3.2. Stabilized Formulation

A standard Galerkin finite element formulation as presented in (50) (or similar finite difference or finite volume strategies) is unstable in the sense that it may produce nonphysical oscillations in regions of steep solution gradients or strong convection. Even when viscous effects are included as in (50) standard Galerkin calculations may produce non-physical oscillations for convection-dominated flows. This well-known phenomenon results because the standard Galerkin formulation (or equivalently

central differencing on a structured grid) produces a difference stencil whose solution admits oscillatory behavior [11–13].

For some classes of flow and transport this instability can be directly related to inadequate spatial resolution in the grid. In these cases the Galerkin discretization on a sufficiently refined mesh will produce stable results. This is typically the case for low-speed incompressible flows for which there is an approximate balance between the convective and diffusive length scales. This balance is described by the cell Reynolds (or Peclet) number, which is defined as

$$Re_c \equiv \frac{\rho U h_{ref}}{\mu} \quad (51)$$

where h_{ref} is the cell reference length and the other properties are evaluated locally. When the local flow properties and mesh spacing is such that $Re_c < 2$ the standard Galerkin formulation will yield non-oscillatory results. Unfortunately, such a balance is rarely achieved for compressible flows in aerospace applications. Indeed, the Euler equations are devoid of any diffusion, so a standard Galerkin discretization such as in Equation (50) will always exhibit stability issues, regardless of mesh resolution.

Several techniques have been proposed to address the stability issue of the Galerkin formulation. The familiar Lax–Wendroff finite difference scheme produces the Taylor–Galerkin scheme in the context of finite elements. The Taylor–Galerkin scheme employs a second-order Taylor series in time and an interchange of spatial and temporal differentiation in the discretization of (44). This yields a second-order term in the discrete form that can be interpreted as a stabilizing diffusion. Recently the Taylor–Galerkin scheme has been applied to hypersonic flowfields in chemical and thermal nonequilibrium [14], illustrating its applicability to the class of problems considered in the present work.

A different approach is pursued by Carey et al. in the Least–Squares finite element method. In the Least–Squares approach the test function \mathbf{W} in (50) is replaced by the variation of the residual of the governing equations [15, 16]. Conceptually this is equivalent to minimizing the residual in a least-squares sense. A detailed analysis of this formulation reveals a stabilizing mechanism similar to the Taylor–Galerkin scheme. This least-squares idea can be combined with the Galerkin statement to yield the so-called Galerkin/least-squares scheme [17].

The stabilization introduced via numerical dissipation in upwind differencing can be achieved in the finite element setting when an upwind bias is added to the test function \mathbf{W} . This idea, and the need to reduce cross-wind dissipation in two or three dimensions, led to the development of the directed streamline–upwind Petrov/Galerkin (SUPG) formulation as another stabilizing mechanism for convection dominated flows [18]. For the system of equations (49) a suitably upstream-biased test function can be defined by augmenting the standard Galerkin test function \mathbf{W} with the convective operator acting on the test function:

$$\hat{\mathbf{W}} = \mathbf{W} + \tau_{\text{SUPG}} \mathbf{A}_i \frac{\partial \mathbf{W}}{\partial x_i} \quad (52)$$

The stabilization matrix τ_{SUPG} plays an important role in the SUPG formulation in that it seeks to introduce the minimal amount of diffusion necessary to stabilize the scheme. In this work τ_{SUPG} is adapted from previous work by Shakib et al [19] in the context of entropy variables and later used by Aliabadi with the conservation variables [20, 21]. Specifically, in three dimensions

$$\tau_{\text{SUPG}} = \text{diag}(\tau_{c,s}, \tau_{m,j}, \tau_E, \tau_{e_V}) \quad (53)$$

where τ_c , $\tau_{m,j}$, τ_E , and τ_{eV} are scalar stabilization parameters for the continuity, momentum, total energy, and vibrational energy equations, respectively, and are given by

$$\begin{aligned}\tau_{c,s} &= \frac{2(\|\mathbf{u}\| + c)}{h_{\text{SUPG}}} \\ \tau_{m,j} &= \left[\left(\frac{2(\|\mathbf{u}\| + c)}{h_{\text{SUPG}}} \right)^2 + \left(\frac{4\mu}{\rho h_{\text{SUPG}}^2} \right)^2 \right]^{-1/2} \\ \tau_E = \tau_{eV} &= \left[\left(\frac{2(\|\mathbf{u}\| + c)}{h_{\text{SUPG}}} \right)^2 + \left(\frac{4k}{\rho c_p h_{\text{SUPG}}^2} \right)^2 \right]^{-1/2}\end{aligned}$$

and are designed to transition smoothly between convective, diffusive, and transient-dominated flow regimes. The flow aligned element length scale, h_{SUPG} , is defined as

$$h_{\text{SUPG}} = C \sqrt{\frac{u_k u_k}{u_i g_{ij} u_j}} \quad (54)$$

where g_{ij} is the covariant metric tensor given by

$$g_{ij} = \frac{\partial \xi_k}{\partial x_i} \frac{\partial \xi_k}{\partial x_j} \quad (55)$$

This definition is clearly a flow aligned length scale once it is realized that the denominator is the norm of the projection of the velocity vector onto the gradient of the computational coordinates.

It is important to note that all of the schemes discussed previously address instabilities induced by strong convection. For supersonic problems involving strong shock waves another form of stabilization is required. More specifically, a local regularization scheme using a shock-capturing function is required to eliminate nonphysical over and under-shoots induced by strong gradients. The regularized SUPG weak statement then follows by multiplying (49) by (52) and integrating by parts as before

$$\begin{aligned}& \int_{\Omega} \left[\mathbf{W} \cdot \left(\frac{\partial \mathbf{U}}{\partial t} + \mathbf{A}_i \frac{\partial \mathbf{U}}{\partial x_i} - \dot{\mathbf{S}} \right) + \frac{\partial \mathbf{W}}{\partial x_i} \cdot \left(\mathbf{K}_{ij} \frac{\partial \mathbf{U}}{\partial x_j} \right) \right] d\Omega \\ & + \sum_{e=1}^{n_{el}} \int_{\Omega_e} \tau_{\text{SUPG}} \frac{\partial \mathbf{W}}{\partial x_k} \cdot \mathbf{A}_k \left[\frac{\partial \mathbf{U}}{\partial t} + \mathbf{A}_i \frac{\partial \mathbf{U}}{\partial x_i} - \frac{\partial}{\partial x_i} \left(\mathbf{K}_{ij} \frac{\partial \mathbf{U}}{\partial x_j} \right) - \dot{\mathbf{S}} \right] d\Omega \\ & + \sum_{e=1}^{n_{el}} \int_{\Omega_e} \delta \left(\frac{\partial \mathbf{W}}{\partial x_i} \cdot \frac{\partial \mathbf{U}}{\partial x_i} \right) d\Omega - \oint_{\Gamma} \mathbf{W} \cdot \mathbf{g} d\Gamma = 0\end{aligned} \quad (56)$$

The shock capturing function is local and essentially regularizes the problem by selectively introducing isotropic artificial diffusion. This added local dissipation captures shocks approximately across a few mesh cells.

The shock capturing function was adapted for a system of conservation variables by LeBeau and Tezduyar [20–22] from the original definition employed by Hughes et al. for the case of entropy variables [19, 23], and is given by

$$\delta_{\text{orig}} = \left[\frac{\left\| \mathbf{A}_i \frac{\partial \mathbf{U}}{\partial x_i} \right\|_{\mathbf{A}_0^{-1}}^2}{\left\| \nabla \xi \cdot \nabla \mathbf{U} \right\|_{\mathbf{A}_0^{-1}}^2 + \left\| \nabla \eta \cdot \nabla \mathbf{U} \right\|_{\mathbf{A}_0^{-1}}^2 + \left\| \nabla \zeta \cdot \nabla \mathbf{U} \right\|_{\mathbf{A}_0^{-1}}^2} \right]^{1/2} \quad (57)$$

where (ξ, η, ζ) are the canonical reference element coordinates and \mathbf{A}_0^{-1} is the mapping from conservation to entropy variables. The physical-domain to reference-domain element transformation terms $(\nabla\xi, \nabla\eta, \nabla\zeta)$ are $\mathcal{O}(1/h)$, hence δ is proportional to h . Thus, in regions of appreciable δ , (56) reduces to an $\mathcal{O}(h)$ approximation of (44) for a piecewise linear finite element approximation.

Note that in (57) the numerator corresponds to the residual of the steady Euler equations, hence (56) is consistent with (44) only for this special case. A modified form is employed in the present work and is defined as

$$\delta = \left[\frac{\left\| \frac{\partial \mathbf{U}}{\partial t} + \mathbf{A}_i \frac{\partial \mathbf{U}}{\partial x_i} - \frac{\partial}{\partial x_i} \left(\mathbf{K}_{ij} \frac{\partial \mathbf{U}}{\partial x_j} \right) \right\|_{\mathbf{A}_0^{-1}}^2}{\left\| \nabla \xi \cdot \nabla \mathbf{U} \right\|_{\mathbf{A}_0^{-1}}^2 + \left\| \nabla \eta \cdot \nabla \mathbf{U} \right\|_{\mathbf{A}_0^{-1}}^2 + \left\| \nabla \zeta \cdot \nabla \mathbf{U} \right\|_{\mathbf{A}_0^{-1}}^2} \right]^{1/2} \quad (58)$$

The time derivative term was absent in the original formulations and has been added here for use in time-accurate simulations. Additionally, the diffusive term in the numerator is included so that consistency with (49) is maintained. That is, this form of the shock capturing parameter will vanish when the discrete solution satisfies (49).

Note that the combination of streamline upwinding and shock capturing required to obtain stable solutions with the finite element method is similar to the upwinding and limiting which is characteristic of total-variation-diminishing (TVD) finite difference and finite volume schemes. TVD schemes typically employ an upwind treatment of the inviscid flux terms which is sufficient to stabilize convective-dominated flows. However, flux or slope-limiters, which are designed to restore monotonicity, are required in the presence of strong shock waves. The shock capturing function used in the present scheme is similar to the use of limiters in that it attempts to restore monotonicity in regions of large gradients such as shock waves. (In general, monotonicity can only be guaranteed for the one-dimensional case.) Both TVD finite volume schemes and the current finite element schemes reduce to first-order at shock waves in an attempt to restore monotonicity of the solution.

3.3. Boundary Conditions

Supersonic and hypersonic viscous and inviscid flows are considered in the subsequent numerical studies. For this class of flows the Navier-Stokes equations form a mixed parabolic-hyperbolic set of partial differential equations. Three classes of boundary conditions relevant to the problem class are supersonic inflow, supersonic outflow, and solid-body boundary conditions.

At supersonic inflow boundaries the characteristics of the system are all directed into the domain, and hence each component of the system may specified as an essential boundary condition. In general, for aerothermodynamic applications the freestream density, velocity, and temperature are usually prescribed. With these primitive variables specified the conservation variables may be determined.

At supersonic outflow boundaries the state is defined entirely by the internal conditions. However, as pointed out by Hauke and Hughes, it is important to include the viscous boundary terms which result from the integration by parts performed in Equation (56) [24]. These boundary term contributions are computed at viscous supersonic outflow boundaries and are included in the system matrix.

In the case of an inviscid flow the solid-body boundary condition reduces to that of no-penetration. For the Navier-Stokes equations, however, at a solid surface the familiar no-slip condition applies, as well as a suitable thermal boundary condition (e.g. isothermal, adiabatic, etc. . .). For more details regarding boundary condition implementation see References 10, 25.

4. Finite Element Formulation

Upon introducing a finite element discretization and corresponding basis to define the approximate solution \mathbf{U}_h and test functions \mathbf{W}_h , and substituting into (56), the corresponding approximate finite element formulation has the form: Find \mathbf{U}_h satisfying the essential boundary and initial conditions such that

$$\begin{aligned} & \int_{\Omega} \left[\mathbf{W}_h \cdot \left(\frac{\partial \mathbf{U}_h}{\partial t} + \mathbf{A}_i \frac{\partial \mathbf{U}_h}{\partial x_i} \right) + \frac{\partial \mathbf{W}_h}{\partial x_i} \cdot \left(\mathbf{K}_{ij} \frac{\partial \mathbf{U}_h}{\partial x_j} \right) - \dot{\mathbf{S}}_h \right] d\Omega \\ & + \sum_{e=1}^{n_{el}} \int_{\Omega_e} \tau_{\text{SUPG}} \frac{\partial \mathbf{W}_h}{\partial x_k} \cdot \mathbf{A}_k \left[\frac{\partial \mathbf{U}_h}{\partial t} + \mathbf{A}_i \frac{\partial \mathbf{U}_h}{\partial x_i} - \frac{\partial}{\partial x_i} \left(\mathbf{K}_{ij} \frac{\partial \mathbf{U}_h}{\partial x_j} \right) - \dot{\mathbf{S}}_h \right] d\Omega \\ & + \sum_{e=1}^{n_{el}} \int_{\Omega_e} \delta \left(\frac{\partial \mathbf{W}_h}{\partial x_i} \cdot \frac{\partial \mathbf{U}_h}{\partial x_i} \right) d\Omega - \oint_{\Gamma} \mathbf{W}_h \cdot \mathbf{g}_h d\Gamma = 0 \end{aligned} \quad (59)$$

for all admissible test functions \mathbf{W}_h .

More specifically, let us expand $\mathbf{U}_h(\mathbf{x}, t)$ and $\mathbf{F}_i(\mathbf{x}, t)$ in terms of the finite element basis functions:

$$\mathbf{U}_h(\mathbf{x}, t) = \sum_j \phi_j(\mathbf{x}) \mathbf{U}_h(\mathbf{x}_j, t) \quad (60)$$

$$\mathbf{F}_i(\mathbf{x}, t) = \sum_j \phi_j(\mathbf{x}) \mathbf{F}_i(\mathbf{x}_j, t) \quad (61)$$

where $\mathbf{U}_h(\mathbf{x}_j, t)$ and $\mathbf{F}_i(\mathbf{x}_j, t) = \mathbf{A}_i(\mathbf{U}_h(\mathbf{x}_j, t)) \mathbf{U}_h(\mathbf{x}_j, t)$ are the nodal solution values and nodal inviscid flux components at time t , respectively. In this work a standard piecewise linear Lagrange basis is chosen for $\{\phi\}$, which yields a nominally second-order accurate scheme. Since the focus here is on supersonic flows which exhibit shock waves no attempt has been made to achieve higher-order spatial discretizations. (As discussed in Section 3.2, the scheme is locally first-order accurate in the vicinity of shocks.) However, previous work with a similar formulation for the compressible Navier–Stokes equations suggests that the current scheme could easily be extended to higher-order for flows without shocks simply by using a higher-order finite element basis [26].

Note the particular discretization chosen in Equation (61) for the inviscid flux term. This approach is motivated by results which show that for the model Burger's equation this grouped discretization yields slightly higher accuracy than the ungrouped scheme [27]. This approach is one of several alternatives presented by Morgan and Peraire for the Galerkin finite element method with the explicit addition of diffusion [28]. Recently this approach has received renewed attention in flux-corrected transport discretizations for multidimensional conservation laws [29, 30]. This treatment has been shown to improve the stability of SUPG formulations for compressible flows, especially when strong shocks are present. For more details see Reference 25.

5. Solution Methodology

Equations (59) form a transient, tightly coupled nonlinear system for the unknown nodal values $\mathbf{U}_h(\mathbf{x}_j, t)$. Even when a steady solution to the governing equations is sought equations (59) are often solved with a pseudo-time continuation strategy. That is, even for steady problems, the unsteady equations are often integrated in time until steady-state is reached. This is especially the case for

compressible flows containing shock waves because strong gradients which occur in the flow imply an extremely small zone of attraction for nonlinear implicit solution schemes such as Newton’s method [31, 32]. Algorithms for solving this type of transient system fall broadly into two categories: explicit and implicit.

Since the present work seeks to use adaptive meshing techniques to locally resolve fine features of the flow (thus decreasing h), the h -dependence of Δt for explicit schemes is particularly unattractive [33]. The cost for this increased stability is the need to solve (at least approximately) a nonlinear implicit system at each time step of the solution. Preconditioned Krylov subspace iterative methods provide a suitable choice of solvers that are amenable to parallel solution and are efficient for the problems of interest here [34].

A standard non-overlapping domain decomposition scheme is used in which a unique set of elements is assigned to each processor used in the simulation (see Reference 35 and references therein). The METIS unstructured graph partitioning library [36] is used to create a weighted partition which attempts to balance the computational load incurred for a hybrid element unstructured mesh.

The domain decomposition approach allows element contributions to the global implicit system to be calculated in parallel. That is, each processor will form the system matrix contributions only for its local elements. These contributions are then accumulated into a distributed sparse matrix data structure, which is ultimately used in an iterative Krylov subspace technique to approximately solve the linear system [10, 35, 37].

As mentioned previously, steady solutions are often found by time-marching the transient governing equations to steady-state. In this sense the initial condition is taken at time $t = 0$ and the solution is marched in time until $\frac{\partial U}{\partial t} \rightarrow 0$. In this way time is essentially a continuation parameter which defines a sequence ($n = 1, 2, \dots$) of solutions U_n which converge to the steady solution U .

The semidiscrete weak form in Equation (59) is discretized in time using backwards finite difference schemes. Both first and second-order accurate in time schemes may be derived from Taylor series expansions in time about $U_h(t_{n+1}) = U_{n+1}$:

$$U_n = U_{n+1} + \frac{\partial U_{n+1}}{\partial t} (t_n - t_{n+1}) + \frac{\partial^2 U_{n+1}}{\partial t^2} \frac{(t_n - t_{n+1})^2}{2} + \mathcal{O}((t_n - t_{n+1})^3)$$

$$U_{n-1} = U_{n+1} + \frac{\partial U_{n+1}}{\partial t} (t_{n-1} - t_{n+1}) + \frac{\partial^2 U_{n+1}}{\partial t^2} \frac{(t_{n-1} - t_{n+1})^2}{2} + \mathcal{O}((t_{n-1} - t_{n+1})^3)$$

These expressions can be manipulated as in [10, 25] to create difference formulas of the form

$$\frac{\partial U_{n+1}}{\partial t} = \alpha_t U_{n+1} + \beta_t U_n + \gamma_t U_{n-1} + \mathcal{O}(\Delta t_{n+1}^p) \tag{62}$$

to yield either a first or second-order accurate scheme. The weights α_t , β_t , and γ_t are given for $p = 1$ and $p = 2$ in Table I.

Table I. First and second-order accurate time discretization coefficients.

p	α_t	β_t	γ_t
1	$\frac{1}{\Delta t_{n+1}}$	$\frac{-1}{\Delta t_{n+1}}$	0
2	$-\beta_t - \gamma_t$	$-\left[\frac{1}{\Delta t_{n+1}} + \frac{1}{\Delta t_n}\right]$	$\frac{\Delta t_{n+1}}{\Delta t_n(\Delta t_{n+1} + \Delta t_n)}$

After time discretization using (62), Equation (59) can be written in residual form for the unknown nodal values $\mathbf{U}_{n+1} \equiv \mathbf{U}_h(t_{n+1})$ as the nonlinear algebraic system

$$\mathbf{R}(\mathbf{U}_{n+1}) = 0 \quad (63)$$

The goal is then to define a sequence of linear problems that, when solved, converge to obtain the solution \mathbf{U}_{n+1} of the nonlinear system (63).

Expanding (63) with a Taylor series about iterate \mathbf{U}_{n+1}^l gives

$$\mathbf{R}(\mathbf{U}_{n+1}^{l+1}) = \mathbf{R}(\mathbf{U}_{n+1}^l) + \left[\frac{\partial \mathbf{R}(\mathbf{U}_{n+1}^l)}{\partial \mathbf{U}_{n+1}} \right] \delta \mathbf{U}_{n+1}^{l+1} + \mathcal{O}\left(\left(\delta \mathbf{U}_{n+1}^{l+1}\right)^2\right) \quad (64)$$

where $\frac{\partial \mathbf{R}}{\partial \mathbf{U}}$ is the Jacobian matrix for the nonlinear system and $\delta \mathbf{U}_{n+1}^{l+1} = \mathbf{U}_{n+1}^{l+1} - \mathbf{U}_{n+1}^l$. Truncating this expansion and setting $\mathbf{R}(\mathbf{U}_{n+1}^{l+1}) = 0$ yields Newton's method

$$0 = \mathbf{R}(\mathbf{U}_{n+1}^l) + \left[\frac{\partial \mathbf{R}(\mathbf{U}_{n+1}^l)}{\partial \mathbf{U}_{n+1}} \right] \delta \mathbf{U}_{n+1}^{l+1} \\ \left[\frac{\partial \mathbf{R}(\mathbf{U}_{n+1}^l)}{\partial \mathbf{U}_{n+1}} \right] \delta \mathbf{U}_{n+1}^{l+1} = -\mathbf{R}(\mathbf{U}_{n+1}^l) \quad (65)$$

which results in an implicit linear system for $\delta \mathbf{U}_{n+1}^{l+1}$ and a sequence of iterates ($l = 0, 1, \dots$) which converges to \mathbf{U}_{n+1} . It is important to recall that Newton's method exhibits second-order *conditional* convergence. That is, the magnitude of $\mathbf{R}(\mathbf{U}_{n+1}^{l+1})$ decreases quadratically at successive iterates provided that the initial guess \mathbf{U}_{n+1}^0 is "sufficiently close" to the unknown \mathbf{U}_{n+1} [38, 39].

While the full-Newton scheme is conceptually simple the implementation is complicated by the nonlinear dependence of the transport properties on the unknowns (see Equations (40)–(41)) and the highly nonlinear nature of the convective terms themselves. In practice, implementing the full-Newton scheme is computationally intensive and, in the case of supersonic flows exhibiting shock waves, is often only of modest benefit. That is, due to the conditional convergence restriction of the method and the sharp gradients or discontinuities which are present in the flowfield, the asymptotic quadratic convergence rate may not be achieved [40]. The implementation of an approximate Newton-Krylov technique to address these issues will be discussed further in the following sections.

The Newton scheme results in a series of sparse linear problems of the form

$$\mathbf{K} \delta \mathbf{U}_{n+1} = \mathbf{f} \quad (66)$$

which must be solved to obtain \mathbf{U}_{n+1} . For the discretization presented in Section 4 using standard piecewise-linear elements \mathbf{K} is a sparse, non-symmetric, non-singular matrix. Given the size and sparseness of \mathbf{K} it is natural to use preconditioned Krylov subspace iterative techniques to approximate $\delta \mathbf{U}_{n+1}$ [41, 42]. The essential kernel of these techniques is the computation of the matrix-vector product $\mathbf{y} = \mathbf{K} \mathbf{x}$. Two techniques for providing this kernel will be discussed, the first stores the sparse matrix and computes the matrix-vector product explicitly; the second computes the action of the matrix-vector product in a "Jacobian-free" sense.

One straightforward technique for solving (66) is to build the system matrix \mathbf{K} and right-hand-side vector \mathbf{f} . Since the matrix is large yet sparse care must be taken to store it efficiently. In the present

work the parallel sparse matrix format implemented in the PETSc toolkit is used, as are the PETSc iterative solvers [37]. When the system matrix is constructed explicitly it may then be copied and modified to serve as a preconditioner as well. In the current work a standard parallel block-Jacobi ILU-0 preconditioner is used [41, 42]. Once the system matrix and preconditioner are formed the required matrix-vector products are computed directly.

A different technique for solving (66) is the so-called Jacobian-free method. Recall from Equation (65) the particular form of the implicit system to be solved:

$$\left[\frac{\partial \mathbf{R}}{\partial \mathbf{U}} \right] \delta \mathbf{U} = -\mathbf{R}(\mathbf{U})$$

For this special case the action of the matrix-vector product $\left[\frac{\partial \mathbf{R}}{\partial \mathbf{U}} \right] \delta \mathbf{U}$ is nothing more than the derivative of \mathbf{R} in the direction specified by $\delta \mathbf{U}$, and may be approximated within $\mathcal{O}(\varepsilon)$ for finite ε as

$$\left[\frac{\partial \mathbf{R}}{\partial \mathbf{U}} \right] \delta \mathbf{U} \approx \frac{\mathbf{R}(\mathbf{U} + \varepsilon \delta \mathbf{U}) - \mathbf{R}(\mathbf{U})}{\varepsilon} \quad (67)$$

From Equation (67) it is clear that the required matrix-vector product may be approximated by differencing successive residual evaluations. It is in this sense that the scheme is matrix-free: the actual system matrix need not be explicitly formed. All that is required is the capability to evaluate the discrete residual $\mathbf{R}(\mathbf{U})$. Of course, for practical applications some form of preconditioning must be applied to the linear system. Depending on the implementation of this preconditioning, the composite scheme may store some approximation of the system matrix. Still, one attractive feature of the matrix-free approach is that it can require substantially less memory than the sparse matrix approach.

Perhaps the most compelling reason to use the matrix-free approach is that it directly yields a quasi-Newton formulation. That is, the finite difference approximation properly accounts for *all* the nonlinearities in the system. This is especially attractive from an algorithm development perspective. For example, alternate shock capturing terms, SUPG weighting functions, equations of state, and transport property definitions can all be implemented simply by defining their contribution to the discrete residual. Their contribution to the quasi-Newton iteration simply falls out through the approximate matrix-vector product (67).

6. Applications

This section presents two applications used to validate the finite element algorithm described in Section 4. Supersonic inviscid and hypersonic, laminar viscous flows in two dimensions are considered here. All computations employ the PETSc toolkit from Argonne National Laboratory [37] to solve the parallel implicit linear systems using the generalized minimum residual (GMRES) Krylov subspace technique [43] with preconditioning. The preconditioner is of parallel block Jacobi-type where each processor sub-block uses an overlapping additive Schwartz method with an incomplete lower-upper factorization at the sub-block level with no fill (ILU-0). Spatial integration is performed with Gauss quadrature rules sufficient to integrate 3rd-order polynomials exactly.

6.1. Dissociating Nitrogen Flow Over A Cylinder

The first example considered is dissociating flow about a two dimensional cylinder at shock tunnel conditions. This configuration was studied experimentally by Hornung and has subsequently formed

the basis for a number of computational studies. The freestream conditions consist of partially dissociated N_2 with a freestream density of $\rho_\infty = 5.349 \times 10^{-3} \text{ kg/m}^3$, temperature of $T_\infty = 1833 \text{ K}$, and velocity of $u_\infty = 5590 \text{ m/s}$. The freestream mass fractions of N_2 and N are 0.927 and 0.073, respectively.

The computational grid for this case is mapped from the unit square $[0, 1] \times [0, 1]$ in the (ξ, η) plane by [44]

$$x(\xi, \eta) = (R_x - (R_x - R_c)\xi) \cos(\theta(2\eta - 1)) \quad (68)$$

$$y(\xi, \eta) = (R_y - (R_y - R_c)\xi) \sin(\theta(2\eta - 1)) \quad (69)$$

where the cylinder radius $R_c = 0.0254 \text{ m}$, the upstream boundary of the computational domain is given by $R_x = 1.75 R_c$, $R_y = 3 R_c$, and $\theta = \frac{5\pi}{12}$. A coarse mesh is shown in Figure 1 with $n_\xi \times n_\eta = 30 \times 60$ elements in the normal and circumferential directions, respectively.

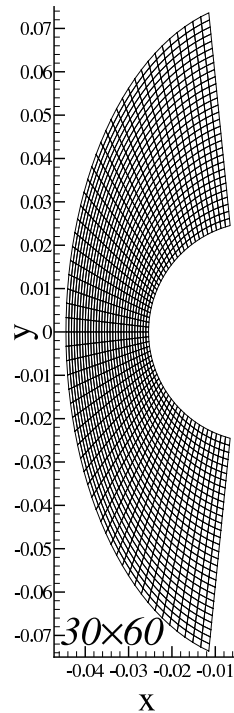


Figure 1. Coarse computational grid for dissociating nitrogen flow over a cylinder

The simulation is initialized with uniform freestream values and marched in time until steady-state is reached. A supersonic inflow boundary condition in which the conserved variables $[\rho_s, \rho u, \rho v, \rho E, \rho e_V]^T$ are specified as essential boundary conditions on the upstream inflow boundary. At the outflow boundary the flow is supersonic, and hence no outflow boundary conditions are specified for this inviscid flow. The no-penetration boundary condition $\mathbf{u} \cdot \hat{\mathbf{n}} = 0$ holds on the cylinder surface

and is enforced as a natural boundary condition through the boundary integral in the weak statement as described in Reference 25.

Figure 2 illustrates the steady-state flowfield for this case. For this inviscid case the governing Euler equations are hyperbolic and admit discontinuous solutions. As expected, the cylinder produces a strong bow shock across which the density, velocity, and pressure jump. Of particular interest is the

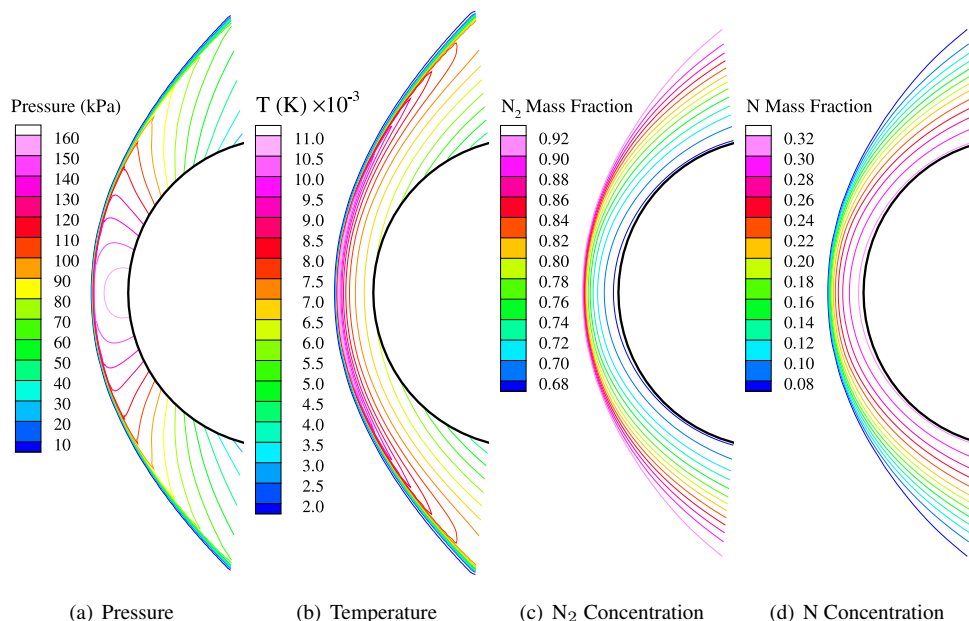


Figure 2. Illustration of flowfield for dissociating nitrogen flow over a cylinder

static temperature field shown in Figure 2(b), which is in sharp contrast to the typical calorically perfect gas result in which the post-shock stagnation region temperature is essentially constant. In this reacting flow the gas reaches temperatures in excess of 11,000 K immediately behind the shock wave. At such extreme temperatures, however, N_2 becomes vibrationally excited and begins to dissociate. This is depicted in Figures 2(c) and 2(d) by the decrease in N_2 and increase in N mass fractions, respectively. (Since there are only two modeled in this case, the species distributions are essentially inverses of each other because of the requirement that everywhere $c_{N_2} + c_N = 1$.)

The behavior for the specific case of the stagnation line is shown more quantitatively in Figure 3, which shows the static temperature and mass fraction distributions along the stagnation line.

The important question of mesh convergence is examined in Figure 4, which depicts static pressure and temperature along the stagnation line for a family of meshes. The coarsest mesh considered, 30×60 elements, is clearly too coarse for this problem, underpredicting the pressure and overpredicting the temperature in the shock layer. It is clear from this coarse mesh, however, that the shock is captured approximately over 3–4 elements. This trend is repeated for all finer meshes. The discrete shockwave is self-similar in this regard because of the lack of physical diffusion in this problem – its thickness is determined solely by the local mesh spacing.

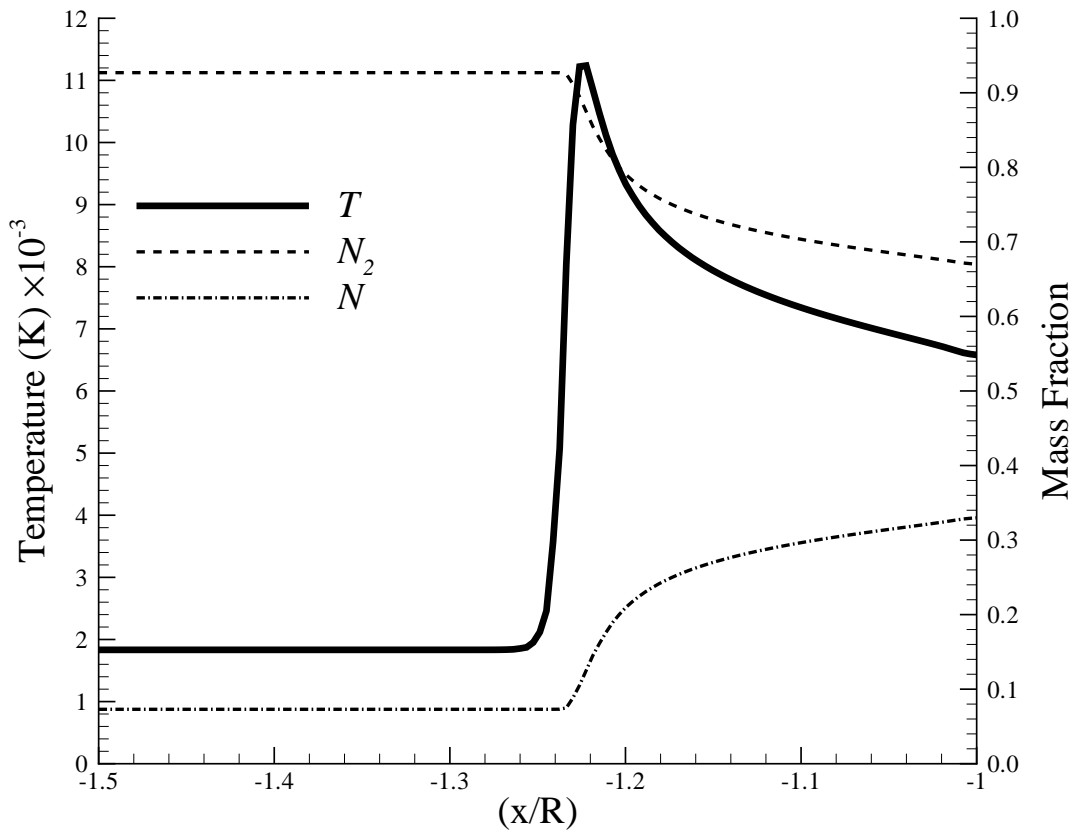


Figure 3. Stagnation line temperature and species mass fractions for inviscid dissociating flow about a cylinder.

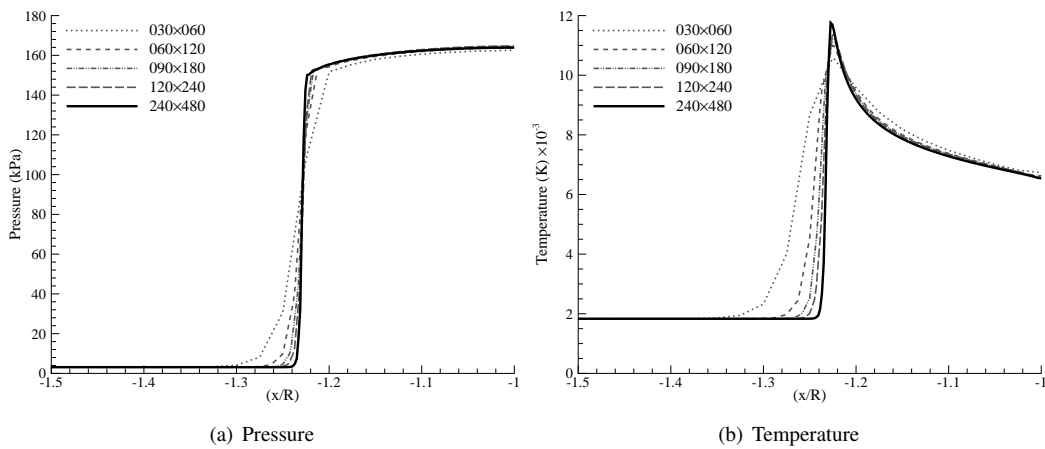


Figure 4. Stagnation line property mesh convergence for dissociating nitrogen flow over a cylinder

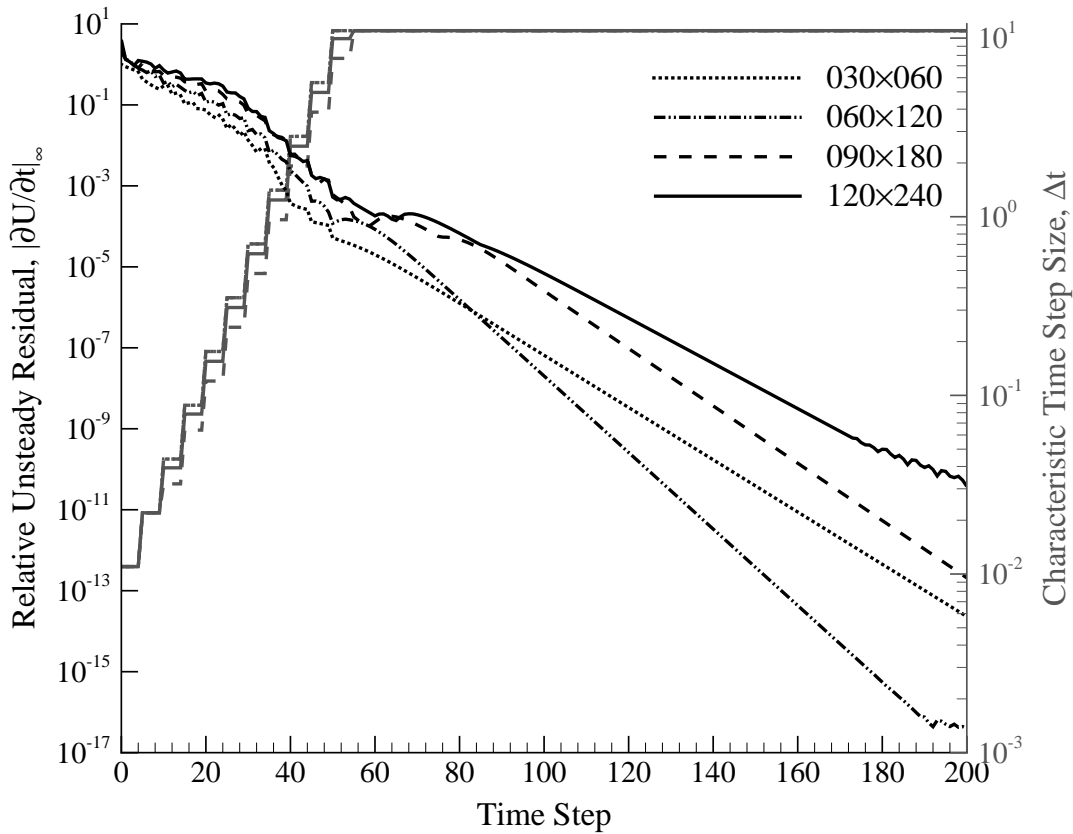


Figure 5. Transient convergence for inviscid dissociating nitrogen flow about a cylinder.

6.2. Dissociating Air Flow Over A Cylinder

A second inviscid case considers dissociating air flow about a cylinder. In this case the reacting gas model contains the five species N_2 , O_2 , NO , N , and O . The freestream mass fractions of N_2 and O_2 are 0.78 and 0.22, respectively. The freestream is characterized by density, velocity, and temperature, whose values are $\rho_\infty = 10^{-3} \text{ kg/m}^3$, $u_\infty = 4.75 \text{ km/sec}$, and $T_\infty = 250 \text{ K}$.

7. Conclusions

A modified finite element formulation is developed to simulate high-Reynolds number flows. The scheme is an extension of the SUPG family augmented by a modified shock capturing operator which is required to eliminate spurious oscillations in the vicinity of shock waves. The main features of this study concern improvements in numerical methodology for compressible Navier-Stokes simulation supported by accompanying verification simulations and an experimental validation study.

The verification test results for Mach 3 flow over a cylinder serves as a good test case for the

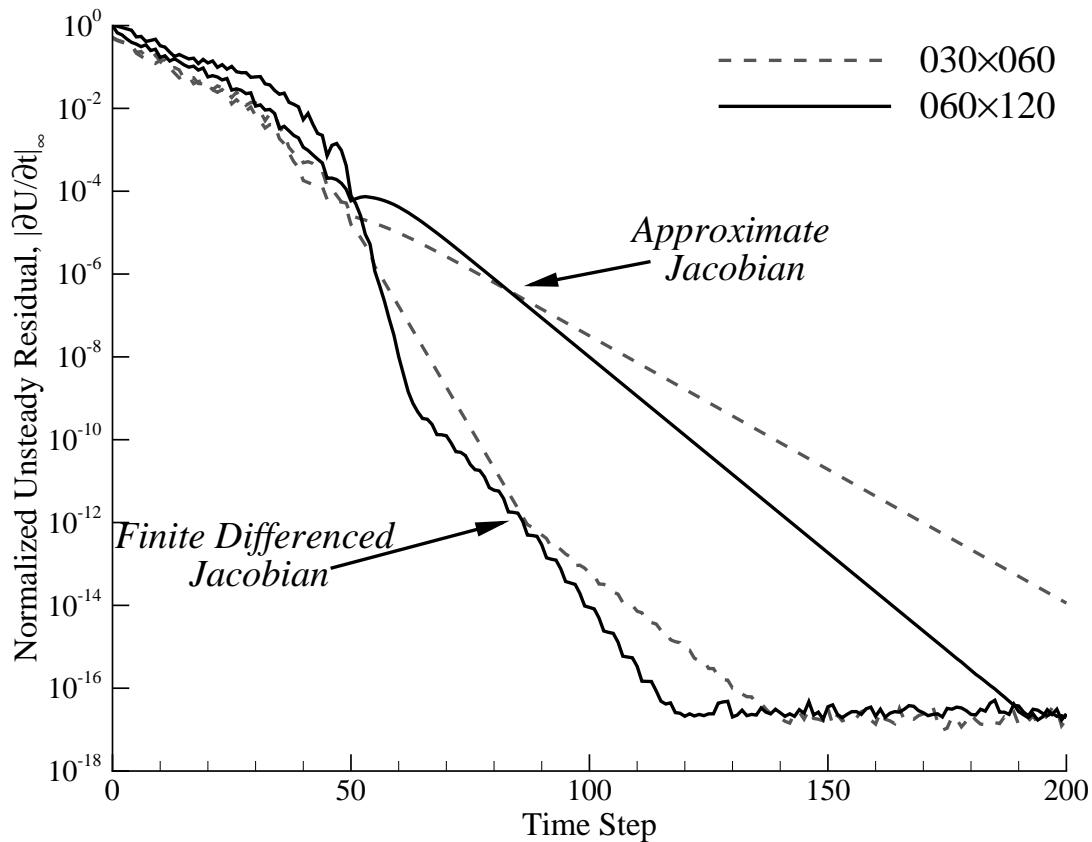


Figure 6. Influence of linearization strategy for inviscid dissociating nitrogen flow about a cylinder.

effectiveness of the modified shock capturing operator (e.g. computed and theoretical jump values are in excellent agreement). The performance of the associated transient, nonlinear, and mesh convergence was investigated. The method was then validated by comparison to experimentally-measured quantities of interest such as surface pressure and heat transfer distributions.

The method is applicable to arbitrary unstructured discretizations, but the results shown here employ high-quality, structured grids. The performance of the algorithm on unstructured meshes, including the influence of mesh quality on solution accuracy, is of interest and will be considered in future work. This is a particularly important question as the ability to use hybrid-element unstructured meshes can greatly simplify the mesh generation process. Additional work will also examine how the specific choice of inviscid flux discretization (Equation (61)) enhances the numerical stability of the method.

While only laminar, calorically perfect gases are considered in this work, the approach is expected to generalize directly to the case of turbulent and/or reacting flows. Future work will extend the range of applicability of the finite element model by including state equations for gases in thermal equilibrium. The effects of turbulence may be included through the typical Reynolds-Averaged Navier-Stokes approach by implementing suitable turbulence models. Additionally, the highly localized shock waves and boundary layers which occur in this class of flows are well-suited for simulation with adaptive

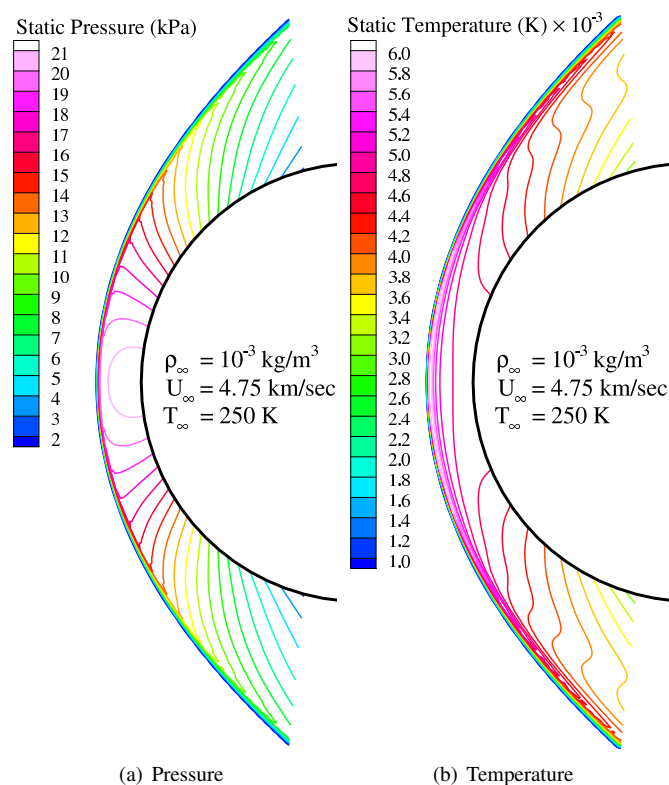


Figure 7. Illustration of flowfield for dissociating air flow over a cylinder

mesh refinement techniques, and such simulations will be the focus of future research.

REFERENCES

1. John D. Anderson, Jr. *Hypersonic and High Temperature Gas Dynamics*. AIAA, Reston, Virginia, 2000.
2. Graham V. Candler. *The Computation of Weakly Ionized Hypersonic Flows in Thermochemical Nonequilibrium*. PhD thesis, Stanford University, June 1988.
3. J. A. Lordi and R. E. Mates. Rotational Relaxation in Nonpolar Diatomic Gas. *Physics of Fluids*, 13(2):291–308, 1970.
4. Chul Park. Rotational Relaxation of N_2 Behind a Strong Shock Wave. *AIAA Journal of Thermophysics and Heat Transfer*, 18(4):527–?, October–December 2004.
5. Peter A. Gnoffo, Roop N. Gupta, and Judy L. Shinn. Conservation equations and physical models for hypersonic air flows in thermal and chemical nonequilibrium. Technical report, National Aeronautics and Space Administration, 1989.
6. Chul Park. *Nonequilibrium Hypersonic Aerothermodynamics*. John Wiley & Sons, 1990.
7. F. G. Blottner, M. Johnson, and M. Ellis. Chemically Reacting Viscous Flow Program for Multi-Component Gas Mixtures. Technical Report Sandia Laboratories Report No. SC-RR-70-754, Sandia National Laboratories, Albuquerque, NM, 1971.
8. Michael J. Wright. *A Family of Data-Parallel Relaxation Methods for the Navier-Stokes Equations*. PhD thesis, The University of Minnesota, June 1997.
9. Vincenti and Kruger. *Introduction to Physical Gas Dynamics*. Krieger, 1965.
10. Benjamin S. Kirk. *Adaptive Finite Element Simulation of Flow and Transport Applications on Parallel Computers*. PhD thesis, The University of Texas at Austin, May 2007.

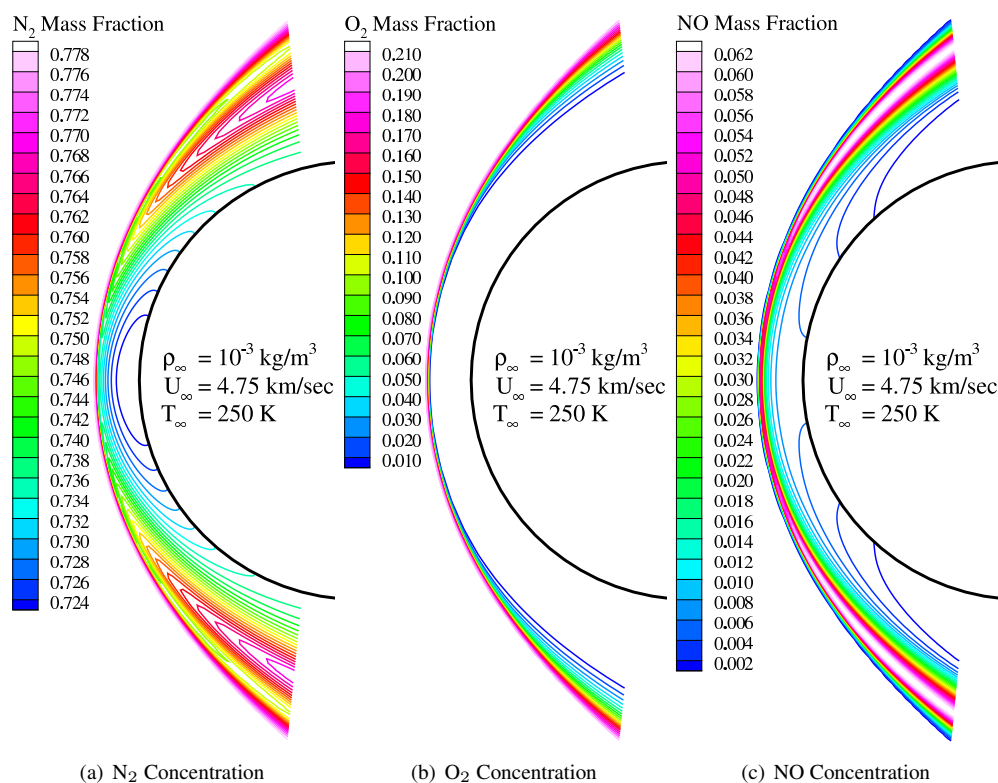


Figure 8. Illustration of flowfield for dissociating air flow over a cylinder: molecular species

11. I. Christie, D. F. Griffiths, A. R. Mitchell, and O. C. Zienkiewicz. Finite element methods for second order differential equations with significant first derivatives. *International Journal for Numerical Methods in Engineering*, 10:1389–1396, 1976.
12. G. F. Carey and J. T. Oden. *Finite Elements: VI, Special Problems in Fluid Mechanics*. Prentice Hall, Englewood Cliffs, 1986.
13. Thomas-Peter Fries and Hermann G. Matthies. A Review of Petrov-Galerkin Stabilization Approaches and an Extension to Meshfree Methods. Technical Report 2004-01, Institute of Scientific Computing, Technical University Braunschweig, March 2004.
14. M. P. Kessler and A. M. Awruch. Analysis of hypersonic flows using finite elements with Taylor-Galerkin scheme. *International Journal for Numerical Methods in Fluids*, 44:1355–1376, 2004.
15. B.N. Jiang and G.F. Carey. A Stable Least-Squares Finite Element Method for Nonlinear Hyperbolic Problems. *International Journal for Numerical Methods in Fluids*, 8:933–942, 1988.
16. B.N. Jiang and G.F. Carey. Least-Squares Finite Element Methods for Compressible Euler Equations. *International Journal for Numerical Methods in Fluids*, 10:557–568, 1990.
17. T. J. R. Hughes, L. P. Franca, and G. M. Hullbert. A new finite element formulation for computational fluid dynamics: VIII. The Galerkin/least-squares method advective-diffusive equations. *Computer Methods in Applied Mechanics and Engineering*, 73:173–189, 1989.
18. T. J. R. Hughes and M. Mallet. A new finite element formulation for computational fluid dynamics: III. the generalized streamline operator for multidimensional advective-diffusive systems. *Computer Methods in Applied Mechanics and Engineering*, 58:305–328, 1986.
19. Farzin Shakib, Thomas J. R. Hughes, and Zdeněk Johan. A new finite element formulation for computational fluid dynamics: X. the compressible Euler and Navier-Stokes equations. *Computer Methods in Applied Mechanics and Engineering*, 100:1–6, 1992.

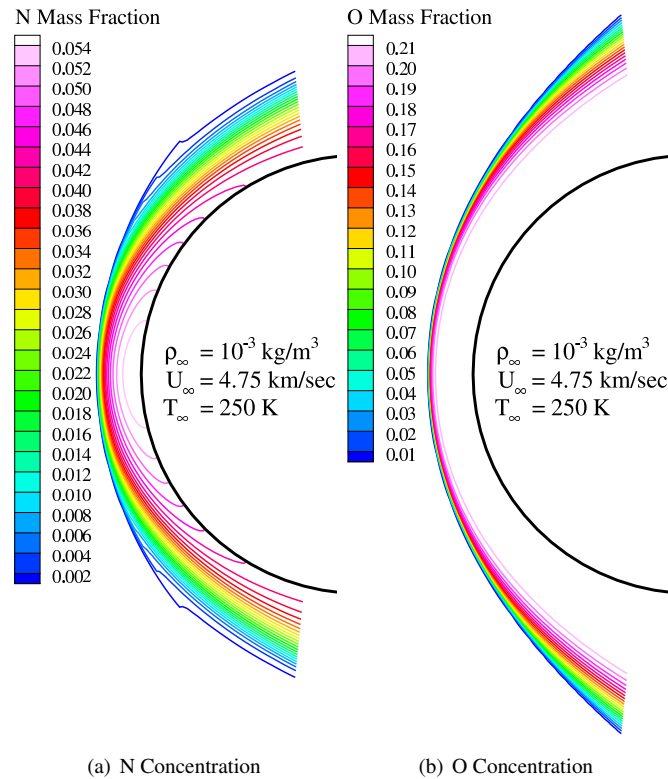


Figure 9. Illustration of flowfield for dissociating air flow over a cylinder: atomic species

- Engineering*, 89:141–219, 1991.
20. S. K. Aliabadi. *Parallel Finite Element Computations in Aerospace Applications*. PhD thesis, The University of Minnesota, 1994.
 21. S. K. Aliabadi and T. E. Tezduyar. Parallel Fluid Dynamics Computations in Aerospace Applications. *International Journal for Numerical Methods in Fluids*, 21:783–805, 1995.
 22. G. J. LeBeau. The Finite Element Computation of Compressible Flows. Master's thesis, The University of Minnesota, 1990.
 23. T. J. R. Hughes and M. Mallet. A new finite element formulation for computational fluid dynamics: IV. a discontinuity operator for multidimensional advective–diffusive systems. *Computer Methods in Applied Mechanics and Engineering*, 58:329–336, 1986.
 24. G. Hauke and T. J. R. Hughes. A comparative study of different sets of variables for solving compressible and incompressible flows. *Computer Methods in Applied Mechanics and Engineering*, 153:1–44, 1998.
 25. Benjamin S. Kirk and Graham F. Carey. Development and Validation of a SUPG Finite Element Scheme for the Compressible Navier-Stokes Equations using a Modified Inviscid Flux Discretization. *International Journal for Numerical Methods in Fluids*, 57(3):265 – 293, 2008.
 26. Daryl Lawrence Bonhaus. *A Higher Order Accurate Finite Element Method for Viscous Compressible Flows*. PhD thesis, Virginia Polytechnic Institute and State University, Blacksburg, VA, November 1998.
 27. C. A. J. Fletcher. The Group Finite Element Formulation. *Computer Methods in Applied Mechanics and Engineering*, 37:225–243, 1983.
 28. K. Morgan and J. Peraire. Unstructured grid finite element methods for fluid mechanics, 1998.
 29. D. Kuzmin, M. Möller, and S. Turek. High-Resolution FEM-FCT Schemes for Multidimensional Conservation Laws. *Computer Methods in Applied Mechanics and Engineering*, 193:4915–4946, May 2004.

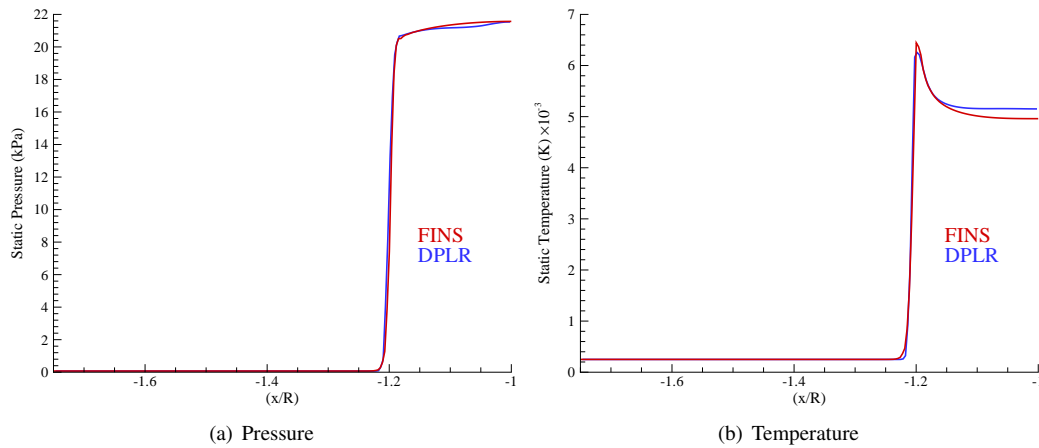


Figure 10. Code-to-code comparison for dissociating air flow over a cylinder – stagnation line pressure and temperature

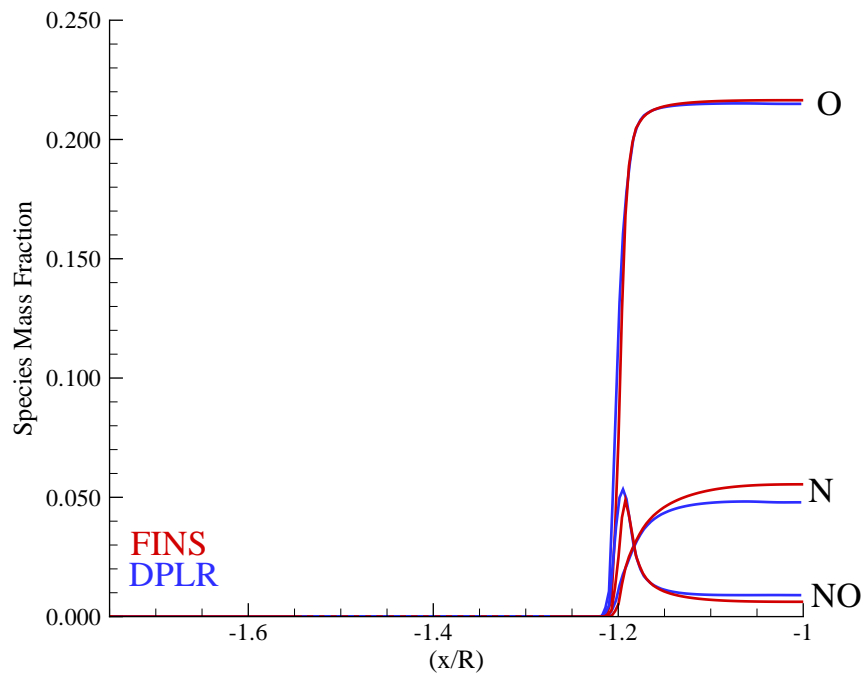


Figure 11. Code-to-code comparison for dissociating air flow over a cylinder – species mass fractions

30. D. Kuzmin and S. Turek. High–Resolution FEM–TVD Schemes Based on a Fully Multidimensional Flux Limiter. *Journal of Computational Physics*, 198:131–158, 2004.
31. W. D. Gropp, D. K. Kaushik, D. E. Keyes, and B. F. Smith. High performance parallel implicit CFD. *Journal of Parallel Computing*, 27:337–362, 2001.
32. P. D. Hovland and L. C. McInnes. Parallel simulation of compressible flow using automatic differentiation and PETSc. *Parallel Computing*, 2000. special issue of Parallel Computing on “Parallel Computing in Aerospace”.
33. J. C. Tannehill, D. A. Anderson, and R. H. Pletcher. *Computational Fluid Mechanics and Heat Transfer*. Taylor & Francis, Washington, D.C., 2nd edition, 1997.
34. D. K. Kaushik, D. E. Keyes, and B. F. Smith. Newton–Krylov–Schwarz methods for aerodynamic problems: Compressible and incompressible flows on unstructured grids. In C.-H. Lai et al., editor, *Proceedings of the 11th International Conference on Domain Decomposition Methods*. Domain Decomposition Press, Bergen, 1999.
35. Benjamin S. Kirk, John W. Peterson, Roy H. Stogner, and Graham F. Carey. libMesh: A C++ Library for Parallel Adaptive Mesh Refinement/Coarsening Simulations. *Engineering with Computers*, 22(3):237–254, 2006.
36. G. Karypis and V. Kumar. METIS unstructured graph partitioning and sparse matrix order. Technical report, University of Minnesota, Department of Computer Science, August 1995.
37. Satish Balay, Kris Buschelman, Victor Eijkhout, William D. Gropp, Dinesh Kaushik, Matthew G. Knepley, Lois Curfman McInnes, Barry F. Smith, and Hong Zhang. PETSc users manual. Technical Report ANL-95/11 - Revision 2.3.0, Argonne National Laboratory, April 2004.
38. A. Iserles. *A first course in the numerical analysis of differential equations*. Cambridge University Press, 1996.
39. Michael D. Greenberg. *Foundations of Applied Mathematics*. Prentice-Hall, 1978.
40. Zdeněk Johan, Thomas J. R. Hughes, and Farzin Shakib. A globally convergent matrix-free algorithm for implicit time-marching schemes arising in finite element analysis in fluids. *Computer Methods in Applied Mechanics and Engineering*, 87:281–304, 1991.
41. R. Barrett, M. Berry, T. F. Chan, J. Demmel, J. M. Donato, Jack Dongarra, V. Eijkhout, R. Pozo, C. Romine, and H. V. der Vorst. *Templates for the Solution of Linear Systems: Building Blocks for Iterative Methods*. Philadelphia: Society for Industrial and Applied Mathematics. Also available as postscript file on <http://www.netlib.org/templates/Templates.html>, 1994.
42. Gene H. Golub and Charles F. Van Loan. *Matrix Computations*. The Johns Hopkins University Press, 3rd edition, 1996.
43. Youcef Saad and Martin H. Schultz. GMRES: a generalized minimal residual algorithm for solving nonsymmetric linear systems. *SIAM Journal on Scientific and Statistical Computing*, 7(3):856–869, 1986.
44. C.-W. Shu. High order finite difference and finite volume WENO schemes and discontinuous Galerkin methods for CFD. Technical Report ICASE Report No. 2001-11, Brown University, Providence, Rhode Island, May 2001.

APPENDIX

I. Model Parameters

In this section we list the parameters employed in the physical models listed in Section 2.

I.1. Chemical & Vibrational Excitation Data

Table II. Chemical Species Physical Parameters

Species	M_s (kg/kmol)	h_s^0 (J/kg) $\times 10^{-6}$	θ_{vs} (K)
N ₂	28.016	0.	3,395.
O ₂	32.000	0.	2,239.
NO	30.008	2.996	2,817.
N	14.008	33.622	–
O	16.000	15.420	–

I.2. Reaction Rates

Table III. Forward Reaction Rate Coefficients (– denotes identical values)

Reaction	\mathcal{M}	C_f m ³ /kmol s	η_r	E_a cal/mol
N ₂ + \mathcal{M} \rightleftharpoons 2N + \mathcal{M}	N ₂	7×10^{18}	–1.6	224,815.2
	O ₂	7×10^{18}	–	–
	NO	7×10^{18}	–	–
	N	3×10^{19}	–	–
	O	3×10^{19}	–	–
O ₂ + \mathcal{M} \rightleftharpoons 2O + \mathcal{M}	N ₂	2×10^{18}	–1.5	118,167.
	O ₂	2×10^{18}	–	–
	NO	2×10^{18}	–	–
	N	1×10^{19}	–	–
	O	1×10^{19}	–	–
NO + \mathcal{M} \rightleftharpoons N + O + \mathcal{M}	N ₂	5×10^{12}	0	149,943.
	O ₂	–	–	–
	NO	–	–	–
	N	–	–	–
	O	–	–	–
N ₂ + O \rightleftharpoons NO + N		6.4×10^{14}	–1	76,262.
NO + O \rightleftharpoons O ₂ + N		8.4×10^9	0	38,628.

1.3. Electronic Excitation

Table IV. Electronic Excitation: Excitation Temperatures & Degeneracies

Species	Degeneracy of the mode	θ_{es}^l (K)	Species	Degeneracy of the mode	θ_{es}^l (K)
N₂	1	0.00000	N	4	0.00000
	3	7.22316×10^4		10	2.76647×10^4
	6	8.57786×10^4		6	4.14931×10^4
	6	8.60503×10^4			
	3	9.53512×10^4			
	1	9.80564×10^4			
	2	9.96827×10^4			
	2	1.04898×10^5			
	5	1.11649×10^5			
	1	1.22584×10^5			
	6	1.24886×10^5			
	6	1.28248×10^5			
	10	1.33806×10^5			
	6	1.40430×10^5			
6	1.50496×10^5				
O₂	3	0.00000	O	5	0.00000
	2	1.13916×10^4		3	2.27708×10^2
	1	1.89847×10^4		1	3.26569×10^2
	1	4.75597×10^4		5	2.28303×10^4
	6	4.99124×10^4		1	4.86199×10^4
	3	5.09227×10^4			
	3	7.18986×10^4			
NO	4	0.00000			
	8	5.46735×10^4			
	2	6.31714×10^4			
	4	6.59945×10^4			
	4	6.90612×10^4			
	4	7.05000×10^4			
	4	7.49106×10^4			
	2	7.62888×10^4			
	4	8.67619×10^4			
	2	8.71443×10^4			
	4	8.88608×10^4			
	4	8.98176×10^4			
	2	8.98845×10^4			
	2	9.04270×10^4			
	2	9.06428×10^4			
	4	9.11176×10^4			

I.4. Blottner Species Viscosity Coefficients

Table V. Species Viscosity Parameters

Species	A_s	B_s	C_s
N ₂	0.0268142	0.317784	-11.3156
O ₂	0.044929	-0.0826158	-9.20195
NO	0.0436378	-0.0335511	-9.57674
N	0.0115572	0.603168	-12.4327
O	0.0203144	0.42944	-11.6031

II. Jacobian Matrices

II.1. Inviscid Flux Jacobians

In this section we derive the inviscid flux Jacobian matrices. Recall

$$\mathbf{U} = \begin{bmatrix} \rho_s \\ \rho u \\ \rho v \\ \rho w \\ \rho E \\ \rho e_V \end{bmatrix}, \quad \mathbf{F}_1 = \begin{bmatrix} \rho_s u \\ \rho u^2 + P \\ \rho uv \\ \rho uw \\ \rho uH \\ \rho ue_V \end{bmatrix}, \quad \mathbf{F}_2 = \begin{bmatrix} \rho_s v \\ \rho vu \\ \rho v^2 + P \\ \rho vw \\ \rho vH \\ \rho ve_V \end{bmatrix}, \quad \mathbf{F}_3 = \begin{bmatrix} \rho_s w \\ \rho wu \\ \rho wv \\ \rho ww + P \\ \rho wH \\ \rho we_V \end{bmatrix}$$

We seek expressions $\mathbf{A}_i \equiv \frac{\partial \mathbf{F}_i}{\partial \mathbf{U}}$. To accomplish this we must express each inviscid flux term as a function of the conserved variables and take the requisite partial derivatives.

$$\frac{\partial}{\partial \mathbf{U}} (\rho_s u_i) :$$

$$\begin{aligned} \rho_s u_i &= \left(\frac{\rho_s}{\rho} \right) \rho u_i \\ &= \left(\frac{\rho_s}{\sum_{r=1}^{ns} \rho_r} \right) \rho u_i \end{aligned}$$

Then

$$\boxed{\frac{\partial}{\partial \rho_r} (\rho_s u_i) = \left(\delta_{sr} - \frac{\rho_s}{\rho} \right) u_i} \quad (70)$$

and

$$\boxed{\frac{\partial}{\partial \rho u_i} (\rho_s u_i) = \frac{\rho_s}{\rho}} \quad (71)$$

The partial derivatives with respect to all other components in \mathbf{U} are zero.

$$\frac{\partial}{\partial \mathbf{U}} (\rho u_i u_j) :$$

$$\begin{aligned} \rho u_i u_j &= \frac{(\rho u_i)(\rho u_j)}{\rho} \\ &= \frac{(\rho u_i)(\rho u_j)}{\sum_{r=1}^{ns} \rho_r} \end{aligned}$$

Then

$$\boxed{\frac{\partial}{\partial \rho_s} (\rho u_i u_j) = -u_i u_j} \quad (72)$$

$$\boxed{\frac{\partial}{\partial \rho u_i} (\rho u_i u_j) = u_j} \quad (73)$$

$$\boxed{\frac{\partial}{\partial \rho u_j} (\rho u_i u_j) = u_i} \quad (74)$$

The partial derivatives with respect to all other components in \mathbf{U} are zero.

$$\frac{\partial P}{\partial \mathbf{U}} :$$

Thermal Nonequilibrium:

$$\begin{aligned} P &= \sum_{s=1}^{ns} \rho_s R_s T \\ &= \rho \left(\sum_{s=1}^{ns} c_s R_s \right) T \\ &= \rho \bar{R} T \end{aligned}$$

Recall that

$$\begin{aligned} \rho E &= \frac{1}{2} \rho (\mathbf{u} \cdot \mathbf{u}) + \sum_{s=1}^{ns} \rho_s C_{v,s}^{\text{tr}} T + \rho e_V + \sum_{r=1}^{ns} \rho_r h_r^0 \\ &= \frac{(\rho u)^2 + (\rho v)^2 + (\rho w)^2}{2\rho} + \rho \bar{C}_v^{\text{tr}} T + \rho e_V + \sum_{r=1}^{ns} \rho_r h_r^0 \\ \rho T &= \frac{1}{\bar{C}_v^{\text{tr}}} \left[\rho E - \frac{(\rho u)^2 + (\rho v)^2 + (\rho w)^2}{2 \sum_{r=1}^{ns} \rho_r} - \rho e_V - \sum_{r=1}^{ns} \rho_r h_r^0 \right] \end{aligned}$$

where $\bar{C}_v^{\text{tr}} = \sum_{s=1}^{ns} c_s C_{v,s}^{\text{tr}}$. The pressure is then given by

$$\begin{aligned} P &= \frac{\bar{R}}{\bar{C}_v^{\text{tr}}} \left[\rho E - \frac{(\rho u)^2 + (\rho v)^2 + (\rho w)^2}{2 \sum_{r=1}^{ns} \rho_r} - \rho e_V - \sum_{r=1}^{ns} \rho_r h_r^0 \right] \\ &= \left(\frac{\sum_{r=1}^{ns} \rho_r R_r}{\sum_{r=1}^{ns} \rho_r C_{v,r}^{\text{tr}}} \right) \left[\rho E - \frac{(\rho u)^2 + (\rho v)^2 + (\rho w)^2}{2 \sum_{r=1}^{ns} \rho_r} - \rho e_V - \sum_{r=1}^{ns} \rho_r h_r^0 \right] \end{aligned} \quad (75)$$

Then

$$\frac{\partial}{\partial \rho_s} (P) = \left(R_s - \frac{C_{v,s}^{\text{tr}} \bar{R}}{\bar{C}_v^{\text{tr}}} \right) T + \frac{\bar{R}}{\bar{C}_v^{\text{tr}}} \left(\frac{1}{2} (u^2 + v^2 + w^2) - h_s^0 \right) \quad (76)$$

$$\frac{\partial}{\partial \rho u_i} (P) = -u_i \frac{\bar{R}}{\bar{C}_v^{\text{tr}}} \quad (77)$$

$$\frac{\partial}{\partial \rho E} (P) = \frac{\bar{R}}{\bar{C}_v^{\text{tr}}} \quad (78)$$

$$\frac{\partial}{\partial \rho e_V} (P) = -\frac{\bar{R}}{\bar{C}_v^{\text{tr}}} \quad (79)$$

Thermal equilibrium: In thermal equilibrium Equation (75) takes on the form

$$\begin{aligned} P &= \left(\frac{\sum_{r=1}^{ns} \rho_r R_r}{\sum_{r=1}^{ns} \rho_r C_{v,r}^{\text{tr}}} \right) \left[\rho E - \frac{(\rho u)^2 + (\rho v)^2 + (\rho w)^2}{2 \sum_{r=1}^{ns} \rho_r} - \rho e_V - \sum_{r=1}^{ns} \rho_r h_r^0 \right] \\ &= \left(\frac{\sum_{r=1}^{ns} \rho_r R_r}{\sum_{r=1}^{ns} \rho_r C_{v,r}^{\text{tr}}} \right) \left[\rho E - \frac{(\rho u)^2 + (\rho v)^2 + (\rho w)^2}{2 \sum_{r=1}^{ns} \rho_r} - \sum_{r=1}^{ns} \rho_r e_s^{\text{vib}}(T) - \sum_{r=1}^{ns} \rho_r e_s^{\text{elec}}(T) - \sum_{r=1}^{ns} \rho_r h_r^0 \right] \end{aligned}$$

Then

$$\frac{\partial P}{\partial \rho_s} = \left(R_s - \frac{C_{v,s}^{\text{tr}} \bar{R}}{\bar{C}_v^{\text{tr}}} \right) T + \frac{\bar{R}}{\bar{C}_v^{\text{tr}}} \left(\frac{1}{2} (u^2 + v^2 + w^2) - e_s^{\text{vib}} - \sum_{r=1}^{ns} \rho_r \frac{\partial e_r^{\text{vib}}}{\partial \rho_s} - e_s^{\text{elec}} - \sum_{r=1}^{ns} \rho_r \frac{\partial e_r^{\text{elec}}}{\partial \rho_s} - h_s^0 \right)$$

Now

$$\begin{aligned} \frac{\partial e_r^{\text{vib}}}{\partial \rho_s} &= \frac{\partial e_r^{\text{vib}}}{\partial T} \frac{\partial T}{\partial \rho_s} \\ &= C_{v,r}^{\text{vib}} \frac{\partial T}{\partial \rho_s} \end{aligned}$$

and it can be shown that

$$\frac{\partial T}{\partial \rho_s} = \frac{1}{\rho \bar{R}} \left(\frac{\partial P}{\partial \rho_s} - T R_s \right)$$

so then

$$\sum_{r=1}^{ns} \rho_r \frac{\partial e_r^{\text{vib}}}{\partial \rho_s} = \frac{\bar{C}_v^{\text{vib}}}{\bar{R}} \left(\frac{\partial P}{\partial \rho_s} - R_s T \right)$$

and similarly

$$\sum_{r=1}^{ns} \rho_r \frac{\partial e_r^{\text{elec}}}{\partial \rho_s} = \frac{C_v^{\text{elec}}}{\bar{R}} \left(\frac{\partial P}{\partial \rho_s} - R_s T \right)$$

which can be used to show

$$\frac{\partial}{\partial \rho_s} (P) = \left(R_s - \frac{C_{v,s}^{\text{tr}}}{\bar{C}_v} \bar{R} \right) T + \frac{\bar{R}}{\bar{C}_v} \left(\frac{1}{2} (u^2 + v^2 + w^2) - e_s^{\text{vib}} - e_s^{\text{elec}} - h_s^0 \right) \quad (80)$$

where $\bar{C}_v = C_v^{\text{tr}} + C_v^{\text{vib}} + C_v^{\text{elec}}$. The remainder of the derivatives are then similar to the nonequilibrium case:

$$\frac{\partial}{\partial \rho u_i} (P) = -u_i \frac{\bar{R}}{\bar{C}_v} \quad (81)$$

$$\frac{\partial}{\partial \rho E} (P) = \frac{\bar{R}}{\bar{C}_v} \quad (82)$$

where \bar{C}_v takes the place of \bar{C}_v^{tr} .

$$\frac{\partial}{\partial U} (\rho u_i H) :$$

$$\begin{aligned} \rho u_i H &= \rho u_i \left(E + \frac{P}{\rho} \right) \\ &= \frac{(\rho u_i) (\rho E + P)}{\rho} \\ &= \frac{(\rho u_i) (\rho E + P)}{\sum_{r=1}^{ns} \rho_r} \\ &= \frac{(\rho u_i) (\rho E)}{\sum_{r=1}^{ns} \rho_r} + \frac{(\rho u_i) P}{\sum_{r=1}^{ns} \rho_r} \end{aligned}$$

Then

$$\frac{\partial}{\partial \rho_s} (\rho u_i H) = \left(\frac{\partial P}{\partial \rho_s} - H \right) u_i \quad (83)$$

$$\frac{\partial}{\partial \rho u_i} (\rho u_i H) = H \quad (84)$$

$$\frac{\partial}{\partial \rho E} (\rho u_i H) = \left(\frac{\partial P}{\partial \rho E} + 1 \right) u_i \quad (85)$$

and

$$\frac{\partial}{\partial \rho e_V} (\rho u_i H) = \frac{\partial P}{\partial \rho e_V} u_i \quad (86)$$

The partial derivatives with respect to all other components in \mathbf{U} are zero.

$$\frac{\partial}{\partial \mathbf{U}} (\rho u_i e_V) :$$

$$\begin{aligned} \rho u_i e_V &= \frac{(\rho u_i)(\rho e_V)}{\rho} \\ &= \frac{(\rho u_i)(\rho e_V)}{\sum_{r=1}^{n_s} \rho_r} \end{aligned}$$

Then

$$\boxed{\frac{\partial}{\partial \rho_s} (\rho u_i e_V) = -u_i e_V} \quad (87)$$

$$\boxed{\frac{\partial}{\partial \rho u_i} (\rho u_i e_V) = e_V} \quad (88)$$

$$\boxed{\frac{\partial}{\partial \rho e_V} (\rho u_i e_V) = u_i} \quad (89)$$

The partial derivatives with respect to all other components in \mathbf{U} are zero.

II.2. Viscous Flux Jacobians

III. Transformation Matrices

III.1. Entropy Variable Transformation Matrix

III.2. Total Enthalpy Shock Capturing Transformation Matrix

Recall that

$$\mathbf{U} = \begin{bmatrix} \rho_s \\ \rho u \\ \rho v \\ \rho w \\ \rho E \\ \rho e_V \end{bmatrix}, \quad \mathbf{V} = \begin{bmatrix} \rho_s \\ \rho u \\ \rho v \\ \rho w \\ \rho H \\ \rho e_V \end{bmatrix} = \begin{bmatrix} \rho_s \\ \rho u \\ \rho v \\ \rho w \\ \rho E + P \\ \rho e_V \end{bmatrix}$$

then the transformation matrix is

$$\mathbf{A}_H = \frac{\partial \mathbf{V}}{\partial \mathbf{U}} = \begin{bmatrix} 1 & 0 & 0 & 0 & 0 & 0 \\ 0 & 1 & 0 & 0 & 0 & 0 \\ 0 & 0 & 1 & 0 & 0 & 0 \\ 0 & 0 & 0 & 1 & 0 & 0 \\ \frac{\partial P}{\partial \rho_s} & \frac{\partial P}{\partial \rho u} & \frac{\partial P}{\partial \rho v} & \frac{\partial P}{\partial \rho w} & \left(1 + \frac{\partial P}{\partial \rho E}\right) & \frac{\partial P}{\partial \rho e_V} \\ 0 & 0 & 0 & 0 & 0 & 1 \end{bmatrix} \quad (90)$$